

# Proportional distribution pattern and modal principle of tuned viscous mass dampers for multi-degree-of-freedom structures

Jianfei Kang<sup>a</sup>, Zhipeng Zhao<sup>b,\*</sup>, Liyu Xie<sup>b</sup>, Chunfeng Wan<sup>c</sup>, Songtao Xue<sup>b,d</sup>

<sup>a</sup> School of Civil Engineering, Suzhou University of Science and Technology, Suzhou, China

<sup>b</sup> Department of Disaster Mitigation for Structures, Tongji University, Shanghai, China

<sup>c</sup> Key Laboratory of Concrete and Prestressed Concrete Structure of Ministry of Education, Southeast University, Nanjing, China

<sup>d</sup> Department of Architecture, Tohoku Institute of Technology, Sendai, Japan

## ARTICLE INFO

### Keywords:

Inerter  
External dissipative systems  
Complex-valued eigenvalue analysis  
Mode-preserving characteristic

## ABSTRACT

A tuned viscous mass damper (TVMD) is an inerter-based damper that has been adopted in several high-rise buildings in earthquake-prone Japan recently to protect the structures from seismic-induced vibrations. However, as a TVMD contains a mass element, it adds degrees of freedom to the controlled structure, making the system's eigenmodes complex. Inspired by the Rayleigh damping matrix, this study proposes a mass-proportionally distributed TVMD (MPD-TVMD) system, which enhances the efficiency of TVMD utilization compared to the previously proposed stiffness-proportionally distributed TVMD (SPD-TVMD) system. It is theoretically proven in this study that when the arrangements of the TVMDs are proportional to the stiffness or mass distribution of the primary structure, the equations of motion of a TVMD controlled shear building can be decomposed into the eigenmodes of the uncontrolled structure. This modal principle allows structural engineers to estimate the response of the controlled structure by understanding the modal characteristics of the uncontrolled system, which is highly beneficial for preliminary design decisions and the retrofitting of existing structures. Furthermore, given that the damping properties at each story level are typically adjusted by the number of dampers installed, it is often unrealistic in practical design to maintain strict proportionality in damper distribution. Through numerical examples, this study demonstrates that TVMD systems with realistic distribution patterns that are slightly different from a strictly proportional distribution can still perform as effectively as strictly proportional systems, providing a comprehensive design basis for the application of inerter-based damper in practical engineering.

## 1. Introduction

Improving passive control technology using inerters to protect structures from damage and undesired vibrations has gained considerable research attention [1–7]. The resistive force generated by a gravitational mass element, is proportional to the absolute acceleration, whereas those of the damping and spring elements are proportional to the relative velocity and displacement between the two terminals, respectively. This renders the analogy between mechanical and electronic networks incomplete. To fill the gap in the force-current analogy between mechanical and electronic networks, Smith [8] defined the inerter as a mass element that generates a resistive force proportional to the relative acceleration between two terminals. Inerter-like devices were proposed before the terminology was proposed. Kawamata [9,10]

proposed a fluid inerter called a mass pump. Fujinami and Yamamoto [11] and Sone *et al.* [12] proposed an inerter-like device using leverage and a pendulum to improve the performance of a dynamic vibration absorber (DVA). Okumura [13,14] developed a vibrational insulator using a rack-and-pinion inerter. The gyro-mass examined by Saitoh [15] is a type of inerter. Arakaki *et al.* [16,17] developed a device that could enhance damping performance using a ball-screw mechanism. However, the apparent mass produced by the ball-screw mechanism was not utilized because its apparent mass amplification effect was insufficient for controlling civil structures. Watanabe *et al.* [2] remodeled the ball-screw device to achieve a large apparent mass exceeding 6000 metric tons, which was later put into practical use in Japan [18,19]. Hwang *et al.* [20] proposed a rotational inertia damper that employs the same mechanism as the ball-screw inerter developed by Watanabe *et al.* To

\* Corresponding author.

E-mail address: [zhaozhipeng@tongji.edu.cn](mailto:zhaozhipeng@tongji.edu.cn) (Z. Zhao).

<https://doi.org/10.1016/j.engstruct.2024.119175>

Received 1 June 2024; Received in revised form 12 August 2024; Accepted 15 October 2024

Available online 24 October 2024

0141-0296/© 2024 Elsevier Ltd. All rights reserved, including those for text and data mining, AI training, and similar technologies.

date, many types of inerter devices have been developed including those using fluids [5,21,22], hydraulics [23], electromagnetic mechanisms [24], and living hinge mechanisms [25].

In addition to the development of various inerter implementation methods, the underlying vibration suppression mechanisms of inerter-based dampers have also been elucidated. Furuhashi and Ishimaru [26] demonstrated that inerters can increase the fundamental natural period of a building structure without changing its mode shapes when the height-wise distribution of the inerters is proportional to the horizontal stiffness of the primary structure. Furthermore, they developed a control strategy to eliminate the participation of the high modes of the structure using a specific height-wise arrangement of inerters. Recognizing the limitations of the conventional tuned mass damper (TMD) in controlling earthquake-induced vibrations due to its reliance on a large gravitational mass [27], Ikago *et al.* [1] proposed the tuned viscous mass damper (TVMD). The TVMD uses an inerter to achieve a large apparent mass with minimal physical mass, enhancing its effectiveness in vibration control. Expanding on this approach, Lazar *et al.* [4,28] introduced the tuned inerter damper (TID), where the damping element is arranged in parallel with a spring, contrasting with the TVMD's configuration, where the damping element is arranged in parallel with the inerter. While the different configurations of TMD and TVMD impact their installation methods, both are designed to optimize energy dissipation through precise tuning. Based on these principles, Ikago *et al.* [1] also derived a closed-form optimal design formula for a TVMD incorporated into a single-degree-of-freedom (SDOF) structure. Consequently, Zhang *et al.* [29] theoretically examined the damping enhancement effect of inerter-based dampers, and elucidated its relationship with the response mitigation effect.

Although simple formulae useful for practicing engineers have been proposed for SDOF systems, their expansion to multiple-degree-of-freedom (MDOF) systems remains challenging. Krenk and Høgsberg [30] considered the influence of non-resonant modes and proposed a two-step design procedure for single inerter-based dampers. In contrast, the balancing principle for multiple distributed inerter-based dampers still needs to be investigated [31]. Using a numerical optimization approach, Taflanidis *et al.* [32] solved a multi-objective optimization problem for the design of MDOF structures equipped with inerter-based dampers. Wen *et al.* [33] synchronously optimized the parameters and placements of tuned-inerter-based dampers using the numerical method. Zhang *et al.* [34] proposed a semi-analytical method for applying the damping enhancement principle to the design of inerter-controlled MDOF systems. Jangid and his co-workers utilized numerical search techniques to obtain the optimal parameters for structures with tuned inerter-based dampers, considering the  $\mathcal{H}_2$  norm, and derived relevant design formulas through curve fitting technique [35,36]. Considering the characteristics of earthquakes and their transient effects on the design parameters of TVMD, Djerouni and his co-workers conducted a systematic study on the numerical optimization of these design aspects [37,38]. These studies provide valuable insights for enhancing the control effectiveness of inerter-based dampers.

Equally important is the need for practical engineers to have access to a straightforward damper design method that does not rely on numerical algorithms, enabling more efficient preliminary design decisions. A promising approach to achieve this is by arranging dampers in a way that allows the modal characteristics of the controlled structure to be quickly understood. Mazza F and Vulcano A [39,40] proposed a simple yet effective 'proportional stiffness criterion' for arranging additional braces and viscoelastic dampers, which led to a displacement-based design method applicable to both steel and concrete structures. They emphasized that because vibration mode shapes remain practically unchanged when braces and/or viscoelastic dampers are added, this criterion is particularly suitable for retrofitting [40]. Similarly, Bruschi E *et al.* [41] applied the 'proportional stiffness criterion' to the distribution of hysteretic dampers and introduced a streamlined design procedure for the seismic upgrade of frame structures. Ikago *et al.*

[42,43] proposed a response approximation method for MDOF systems containing TVMDs, based on the assumption that uncontrolled mode shapes provide a good approximation of controlled mode shapes when the height-wise TVMD distribution is close to the stiffness distribution of the primary structure. Numerical case studies [34,42–45] have suggested that well-designed TVMDs incorporated into a building structure practically preserve uncontrolled modes, validating the response approximation method. However, the scope of these studies on inerter-based device arrangements is limited to their installation between adjacent floors, and they do not provide a clear theoretical basis for approximating the mode shapes of TVMD controlled shear buildings using uncontrolled mode shapes. Given the promising application of TVMDs for complex structures, the easy-to-understand design principle and installation criterion is required for the inerter-based control technology in practical engineering.

Inspired by the physical implementation of the Rayleigh damping matrix [46–48], this study identifies a novel proportional distribution form for installing TVMDs between floors and the ground, namely the mass-proportionally distributed TVMD (MPD-TVMD). Along with the previously studied stiffness-proportionally distributed TVMD (SPD-TVMD), this research aims to establish a comprehensive distribution pattern and corresponding modal principles for TVMDs in multi-degree-of-freedom (MDOF) structures. Initially, the governing equations,  $\mathcal{H}_\infty$  optimal design method, and eigenvalue analysis for SDOF structures containing a TVMD were reviewed. Following this, methods for implementing stiffness- and mass-proportional damping systems using TVMDs were introduced, along with unified governing equations. The modal participation vectors of MDOF systems controlled by these TVMDs were then constructed to explore the relationship between the participation mode vectors of the uncontrolled and TVMD controlled structures. Finally, analytical examples were employed to validate the modal principles of SPD-TVMD and MPD-TVMD systems. The impact of deviations from the ideal distribution patterns due to practical arrangement issues, as well as the efficiency of SPD- and MPD-TVMD in utilizing TVMDs, were also thoroughly discussed.

## 2. SDOF structures containing a TVMD

This section reviews the equations of motion for a SDOF structures containing a TVMD [1] and the  $\mathcal{H}_\infty$  optimal design method [49], providing straightforward design formulas for the proportionally distributed TVMDs in the following sections. Through eigenvalue analysis of SDOF structures incorporating a TVMD, this section defines the equations for the complex mode vectors in TVMD controlled SDOF structures, thereby establishing a foundational basis for the theoretical exploration in Section 3 of the relationship between the participation mode vectors of uncontrolled and TVMD controlled MDOF structures.

### 2.1. Equations of motion and $\mathcal{H}_\infty$ optimal design

The incorporation of a TVMD into an SDOF structure adds one DOF yielding a 2-DOF system, as shown in Fig. 1(a). The equations of motion of the 2-DOF system subjected to ground acceleration  $\ddot{x}_0$  can be expressed as follows:

$$\widehat{\mathbf{M}}\ddot{\widehat{\mathbf{x}}} + \widehat{\mathbf{C}}\dot{\widehat{\mathbf{x}}} + \widehat{\mathbf{K}}\widehat{\mathbf{x}} = -\widehat{\mathbf{M}}\bar{\Gamma}\ddot{x}_0 \quad (1)$$

where,

$$\widehat{\mathbf{M}} = \begin{bmatrix} m & 0 \\ 0 & m_d \end{bmatrix}, \widehat{\mathbf{C}} = \begin{bmatrix} c & 0 \\ 0 & c_d \end{bmatrix}, \widehat{\mathbf{K}} = \begin{bmatrix} k + k_b & -k_b \\ -k_b & k_b \end{bmatrix}, \widehat{\mathbf{x}} = \begin{Bmatrix} x \\ x_d \end{Bmatrix}, \bar{\Gamma} = \begin{Bmatrix} 1 \\ 0 \end{Bmatrix}. \quad (2)$$

$x$  and  $x_d$  are the displacements of the primary system and the inerter, respectively.  $m$ ,  $c$ , and  $k$  denote the mass, damping coefficient, and

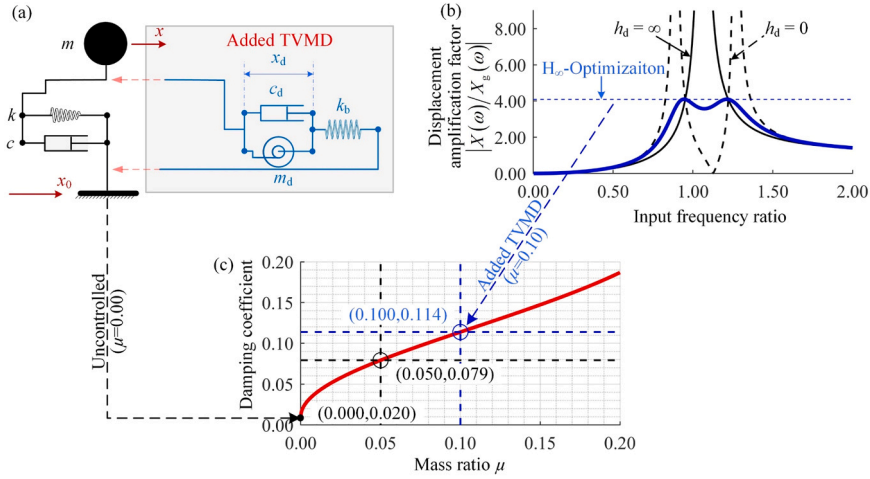


**Fig. 1.** Single-degree-of-freedom (SDOF) structure controlled by tuned viscous mass damper (TVMD): (a) Schematic of an uncontrolled SDOF structure and its configuration after TVMD installation. (b)  $\mathcal{H}_\infty$  optimization concept, illustrating the minimization of peak displacement amplification factor through fixed points on the controlled structure's response curves. (c) Enhancement of the damping coefficient through TVMD installation, demonstrating increased damping effect with higher mass ratio  $\mu$ .

stiffness of the primary system, respectively.  $m_d$ ,  $c_d$ , and  $k_b$  denote the apparent mass, supporting spring stiffness, and damping coefficient of the TVMD, respectively.

Dividing both sides of Eq. (1) by  $m$  yields:

$$\begin{aligned} \ddot{x} + 2h\omega_0\dot{x} + (1 + \eta)\omega_0^2x - \eta\omega_0^2x_d &= -\ddot{x}_0 \\ \mu\ddot{x}_d + 2\mu\beta h_d\omega_0\dot{x}_d - \eta\omega_0^2x + \eta\omega_0^2x_d &= 0 \end{aligned} \quad (3)$$

where,

$$\begin{aligned} \mu &= \frac{m_d}{m}, \quad \omega_0 = \sqrt{\frac{k}{m}}, \quad \omega_d = \sqrt{\frac{k_b}{m_d}}, \quad h = \frac{c}{2\sqrt{mk}}, \quad h_d = \frac{c_d}{2\sqrt{m_d k_b}}, \quad \beta = \frac{\omega_d}{\omega_0}, \quad \eta \\ &= \frac{k_b}{k} \end{aligned} \quad (4)$$

As illustrated in Fig. 1(b), considering the goal to minimize the peak of the displacement amplification factor of a SDOF system containing a TVMD, namely through the  $\mathcal{H}_\infty$  optimization in the frequency domain, Saito *et al.* [49] derived the following closed-form design formulas:

$$\beta^o = \frac{1 - \sqrt{1 - 4\mu}}{2\mu}, \quad h_d^o = \frac{\sqrt{3(1 - \sqrt{1 - 4\mu})}}{4}, \quad \eta^o = \mu(\beta^o)^2 \quad (5)$$

where the superscript ‘‘o’’ denotes the optimum design.

By substituting the optimal solutions  $\beta^o$ ,  $h_d^o$  and  $\eta^o$  from Eq. (5) into Eq. (4), the equations for the supporting spring stiffness and damping coefficient of the TVMD are obtained in terms of the apparent mass of the TVMD:

$$c_d = 2\beta^o h_d^o \omega_0 m_d, \quad k_d = (\beta^o)^2 \omega_0^2 m_d \quad (6)$$

Hence, the correlation between the mass ratio  $\mu$  and the added damping coefficient of the target mode resulting from the installation of a TVMD can be concluded in Fig. 1(c). For example, a TVMD with a mass ratio  $\mu = 0.1$ , when installed in a damped SDOF structure, increases the damping coefficient of the targeted mode from an inherent damping value of 0.02 to a damped condition of 0.114.

## 2.2. Eigenvalue analysis of SDOF structure containing TVMD

The second-order differential equation, Eq. (1), is reduced to a first-order differential equation as follows:

$$\mathbf{A}\dot{\mathbf{z}} + \mathbf{Bz} = \mathbf{A}\mathbf{w}\ddot{x}_0 \quad (7)$$

where

$$\mathbf{z} = \begin{Bmatrix} \dot{\mathbf{x}} \\ \mathbf{x} \end{Bmatrix}, \mathbf{A} = \begin{bmatrix} \mathbf{O} & \widehat{\mathbf{M}} \\ \widehat{\mathbf{M}} & \widehat{\mathbf{C}} \end{bmatrix}, \mathbf{B} = \begin{bmatrix} -\widehat{\mathbf{M}} & \mathbf{O} \\ \mathbf{O} & \widehat{\mathbf{K}} \end{bmatrix}, \mathbf{w} = \begin{Bmatrix} \bar{\mathbf{r}} \\ \mathbf{0} \end{Bmatrix} \quad (8)$$

The characteristic equation for the 2-DOF system is

$$|\lambda\mathbf{A} + \mathbf{B}| = 0 \quad (9)$$

Provided that this non-classically damped system is underdamped, Eq. (9) yields two pairs of complex conjugate eigenvalues  $\lambda_\ell, \lambda_\ell^*$  ( $\ell = 1, 2$ ) and the corresponding eigenvectors can be expressed as  $\boldsymbol{\phi}_\ell = \{\phi_\ell, \phi_{d,\ell}\}^T$ ,  $\boldsymbol{\phi}_\ell^* = \{\phi_\ell^*, \phi_{d,\ell}^*\}^T$ , where  $()^*$  denotes the complex conjugate. Thus, based on the definition of eigenvalues for a non-classically damped system, substituting  $\mathbf{x} = \phi_\ell e^{\lambda_\ell t}$ ,  $\mathbf{x}_d = \phi_{d,\ell} e^{\lambda_\ell t}$  and  $\mathbf{x} = \phi_\ell^* e^{\lambda_\ell^* t}$ ,  $\mathbf{x}_d = \phi_{d,\ell}^* e^{\lambda_\ell^* t}$  into Eq. (3) yields the following equations for ( $\ell = 1, 2$ ):

$$\begin{aligned} \lambda_\ell^2 \phi_\ell + 2h\omega_0 \lambda_\ell \phi_\ell + (1 + \eta^o)\omega_0^2 \phi_\ell - \eta^o \omega_0^2 \phi_{d,\ell} &= 0 \\ \mu \lambda_\ell^2 \phi_{d,\ell} + 2\mu\beta^o h_d^o \omega_0 \lambda_\ell \phi_{d,\ell} - \eta^o \omega_0^2 \phi_\ell + \eta^o \omega_0^2 \phi_{d,\ell} &= 0 \end{aligned} \quad (10)$$

$$\begin{aligned} \lambda_\ell^{*2} \phi_\ell^* + 2h\omega_0 \lambda_\ell^* \phi_\ell^* + (1 + \eta^o)\omega_0^2 \phi_\ell^* - \eta^o \omega_0^2 \phi_{d,\ell}^* &= 0 \\ \mu \lambda_\ell^{*2} \phi_{d,\ell}^* + 2\mu\beta^o h_d^o \omega_0 \lambda_\ell^* \phi_{d,\ell}^* - \eta^o \omega_0^2 \phi_\ell^* + \eta^o \omega_0^2 \phi_{d,\ell}^* &= 0 \end{aligned} \quad (11)$$

It is worth noting that, despite their relative complexity, Eqs. (10) and (11) represent the same characteristic equation for the 2-DOF system as Eq. (9). These equations can also be directly used to solve for the complex conjugate eigenvalues  $\lambda_\ell, \lambda_\ell^*$  ( $\ell = 1, 2$ ) and the corresponding eigenvectors [50].

Let  $v_\ell$  and  $v_\ell^*$  denote participation factors of  $\boldsymbol{\phi}_\ell$  and  $\boldsymbol{\phi}_\ell^*$ , the following relationship holds:

$$\sum_{\ell=1}^2 (v_\ell \boldsymbol{\phi}_\ell + v_\ell^* \boldsymbol{\phi}_\ell^*) = \bar{\mathbf{r}} \quad (12)$$

$$v_\ell = \frac{m\phi_\ell}{m\phi_\ell^2 + m_d\phi_{d,\ell}^2}, v_\ell^* = \frac{m\phi_\ell^*}{m\phi_\ell^{*2} + m_d\phi_{d,\ell}^{*2}} \quad (13)$$

## 3. MDOF shear buildings containing proportionally distributed TVMDs

Despite the emergence of various optimization methods to enhance the vibration control efficiency of TVMDs, the addition of mass elements in a TVMD increases the degrees of freedom in the controlled structure, complicating the system's characteristics for engineers to manage.

Therefore, finding a reasonable distribution to simplify this complexity is desirable. In this section, two types of proportionally distributed TVMDs, with their installation methods illustrated in Fig. 2, are examined. The apparent masses of the TVMDs are proportionally distributed according to either the primary stiffness or mass, referred to as stiffness-proportionally distributed TVMD (SPD-TVMD) and mass-proportionally distributed TVMD (MPD-TVMD), respectively. First, a transfer matrix is employed to unify the governing equations of these TVMD controlled systems. Then, the modal participation vectors of MDOF systems controlled by these TVMDs are constructed to explore the unique modal principles arising from these distribution patterns.

### 3.1. Equations of motion

The mass and stiffness of the  $j$ -th story of the primary structure are denoted as  $m_j$  and  $k_j$ . The displacement of the  $j$ -th story relative to the ground is denoted by  $x_j$ . The equation of motion of the uncontrolled structure can be expressed as follows:

$$\mathbf{M}_p \ddot{\mathbf{x}} + \mathbf{C}_p \dot{\mathbf{x}} + \mathbf{K}_p \mathbf{x} = -\mathbf{M}_p \mathbf{r} \ddot{x}_0 \quad (14)$$

where

$$\mathbf{x} = \{x_1, x_2, \dots, x_n\}^T, \quad \mathbf{r} = \{1, 1, \dots, 1\}^T \quad (15)$$

$$\mathbf{M}_p = \text{diag}(m_1, m_2, \dots, m_n) \quad (16)$$

$$\mathbf{K}_0 = \text{diag}(k_1, k_2, \dots, k_n) \quad (17)$$

$$\mathbf{K}_p = \mathbf{T}^T \mathbf{K}_0 \mathbf{T} \quad (18)$$

$\mathbf{T}$  is the  $n \times n$  ordinate transformation matrix that transforms the relative displacements into interstory drifts.

$$\mathbf{T} = \begin{bmatrix} 1 & 0 & \dots & 0 \\ -1 & 1 & & \\ 0 & \ddots & \ddots & \vdots \\ \vdots & & -1 & 1 & 0 \\ 0 & \dots & 0 & -1 & 1 \end{bmatrix} \quad (19)$$

Hence, the equation of motion of the system shown in Fig. 2 can be expressed as follows [43]:

$$\tilde{\mathbf{M}} \ddot{\tilde{\mathbf{x}}} + \tilde{\mathbf{C}} \dot{\tilde{\mathbf{x}}} + \tilde{\mathbf{K}} \tilde{\mathbf{x}} = -\tilde{\mathbf{M}} \tilde{\mathbf{r}} \ddot{x}_0 \quad (20)$$

where  $\tilde{\mathbf{M}}$ ,  $\tilde{\mathbf{C}}$ , and  $\tilde{\mathbf{K}}$  are the mass, damping, and stiffness matrices of the MDOF shear building containing distributed TVMDs, respectively.

$$\tilde{\mathbf{x}} = \begin{Bmatrix} \mathbf{x} \\ \mathbf{x}_d \end{Bmatrix}, \quad \tilde{\mathbf{M}} = \begin{bmatrix} \mathbf{M}_p & \mathbf{0} \\ \mathbf{0} & \mathbf{M}_D \end{bmatrix}, \quad \tilde{\mathbf{C}} = \begin{bmatrix} \mathbf{C}_p & \mathbf{0} \\ \mathbf{0} & \mathbf{C}_D \end{bmatrix}, \quad \tilde{\mathbf{K}} = \begin{bmatrix} \mathbf{K}_p + \mathbf{K}_{B11} & \mathbf{K}_{B12} \\ \mathbf{K}_{B21} & \mathbf{K}_{B22} \end{bmatrix} \quad (21)$$

$$\mathbf{M}_D = \text{diag}(m_{d,1}, m_{d,2}, \dots, m_{d,n}) \quad (22)$$

$$\mathbf{C}_D = \text{diag}(c_{d,1}, c_{d,2}, \dots, c_{d,n}) \quad (23)$$

$$\mathbf{K}_B = \text{diag}(k_{b,1}, k_{b,2}, \dots, k_{b,n}) \quad (24)$$

$$\mathbf{K}_{B11} = \mathbf{T}_c^T \mathbf{K}_B \mathbf{T}_c, \quad \mathbf{K}_{B12} = -\mathbf{T}_c^T \mathbf{K}_B, \quad \mathbf{K}_{B21} = \mathbf{K}_{B12}^T, \quad \mathbf{K}_{B22} = \mathbf{K}_B \quad (25)$$

$$\tilde{\mathbf{r}} = \{\mathbf{r}^T, 0, 0, \dots, 0\}^T \quad (26)$$

$\mathbf{x}_d = \{x_{d,1}, x_{d,2}, \dots, x_{d,n}\}^T$  denote the relative displacement between the two terminals of the inerters.  $m_{d,j}$ ,  $c_{d,j}$ ,  $k_{b,j}$  represent the apparent mass, damping coefficient, and tuning spring stiffness of the TVMD corresponding to the  $j$ -th story, respectively.

To ensure that the uncontrolled structure decouples into independent equations of motion while maintaining reasonable damping characteristics within a certain range, the damping matrix is assumed to be of Rayleigh type, which is a linear combination of the mass and stiffness matrices:

$$\mathbf{C}_p = \alpha_M \mathbf{M}_p + \alpha_K \mathbf{K}_p \quad (27)$$

where,  $\alpha_M$  and  $\alpha_K$  denote the mass-proportional and stiffness-proportional damping coefficient, respectively.  $\mathbf{T}_c$  is the  $n \times n$  coordinate transformation matrix that transforms the relative displacements of the primary structure into deformations of the TVMDs.

In the case of interstory-installed TVMDs (Fig. 2(a)), of which SPD-TVMD is a special case,  $\mathbf{T}_c$  can be expressed as

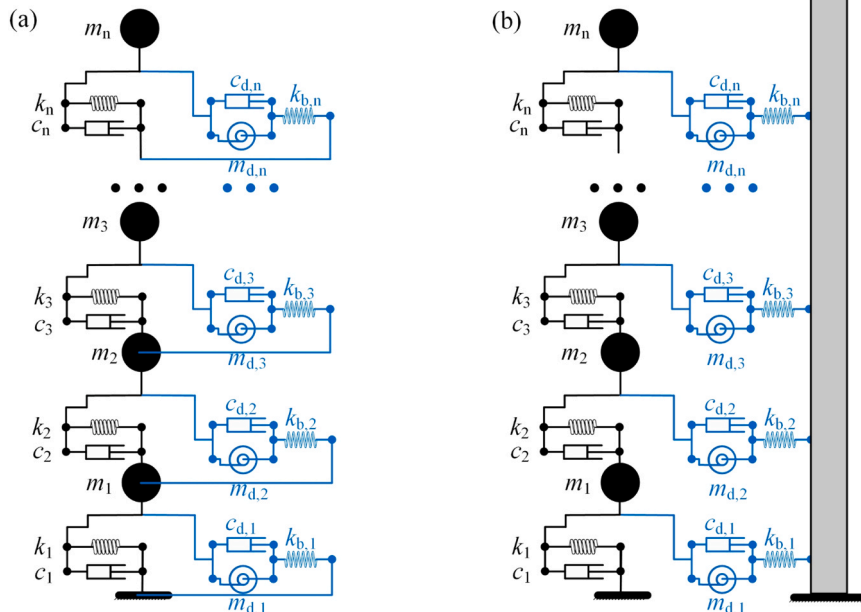


Fig. 2. Two TVMD controlled multiple-degree-of-freedom (MDOF) Systems: (a) Interstory-installed TVMDs. (b) Grounded-installed TVMDs.

$$\mathbf{T}_c = \begin{bmatrix} 1 & 0 & \cdots & 0 \\ -1 & 1 & & \\ 0 & \ddots & \ddots & \vdots \\ \vdots & & -1 & 1 & 0 \\ 0 & \cdots & 0 & -1 & 1 \end{bmatrix} = \mathbf{T} \quad (28)$$

When TVMDs are installed between the floor and ground, as shown in Fig. 2(b), of which MPD-TVMD is a special case,  $\mathbf{T}_c$  is the identity matrix of size  $n$ .

$$\mathbf{T}_c = \text{diag}(1, 1, \dots, 1) \quad (29)$$

For SPD-TVMD system, combining with the Eq. (6), the following equation holds for interstory-installed TVMDs when all TVMDs are tuned to the first mode:

$$m_{d,j} = \alpha k_j \quad (30)$$

$$c_{d,j} = 2\beta^\circ h_d^\circ \omega_1 m_{d,j} = 2\alpha\beta^\circ h_d^\circ \omega_1 k_j \quad (31)$$

$$k_{d,j} = (\beta^\circ)^2 \omega_1^2 m_{d,j} = \alpha(\beta^\circ)^2 \omega_1^2 k_j \quad (32)$$

where,  $\alpha$  is the scaling factor, and  $\omega_1$  is the first fundamental angular frequency of the uncontrolled structure.

Then,

$$\mathbf{M}_D = \alpha \mathbf{K}_0 \quad (33)$$

$$\mathbf{C}_D = 2\beta^\circ h_d^\circ \omega_1 \mathbf{M}_D = 2\alpha\beta^\circ h_d^\circ \omega_1 \mathbf{K}_0 \quad (34)$$

$$\mathbf{K}_B = (\beta^\circ \omega_1)^2 \mathbf{M}_D = \alpha(\beta^\circ \omega_1)^2 \mathbf{K}_0 \quad (35)$$

$$\mathbf{K}_{B11} = \mathbf{T}^T \mathbf{K}_B \mathbf{T} = \alpha(\beta^\circ \omega_1)^2 \mathbf{K}_p \quad (36)$$

Similarly, for MPD-TVMD system, combining with the Eq. (6), the following equation holds when TVMDs are installed between the floor and ground and all TVMDs are tuned to the first mode:

$$m_{d,j} = \alpha m_j \quad (37)$$

$$c_{d,j} = 2\beta^\circ h_d^\circ \omega_1 m_{d,j} = 2\alpha\beta^\circ h_d^\circ \omega_1 m_j \quad (38)$$

$$k_{d,j} = (\beta^\circ)^2 \omega_1^2 m_{d,j} = \alpha(\beta^\circ)^2 \omega_1^2 m_j \quad (39)$$

Then,

$$\mathbf{M}_D = \alpha \mathbf{M}_p \quad (40)$$

$$\mathbf{C}_D = 2\beta^\circ h_d^\circ \omega_1 \mathbf{M}_D = 2\alpha\beta^\circ h_d^\circ \omega_1 \mathbf{M}_p \quad (41)$$

$$\mathbf{K}_B = (\beta^\circ \omega_1)^2 \mathbf{M}_D = \alpha(\beta^\circ \omega_1)^2 \mathbf{M}_p \quad (42)$$

$$\mathbf{K}_{B11} = \mathbf{K}_B = \alpha(\beta^\circ \omega_1)^2 \mathbf{M}_p \quad (43)$$

### 3.2. Theoretical proof of modal principles

For typical building structures, their eigen-vectors are linearly independent [50]. Consequently, an arbitrary displacement vector of a  $n$ -DOF primary structure,  $\mathbf{x}$  can be expressed by a linear combination of the eigen-vectors of the uncontrolled primary system  $\mathbf{u}_j$  ( $j = 1 \dots n$ ) [51]:

$$\mathbf{x} = \sum_{j=1}^n \xi_j \mathbf{u}_j \quad (44)$$

where  $\xi_j$  denotes the  $j$ -th modal coordinate of the primary system.

Note that the matrix  $\mathbf{T}_c$  is invertible, vectors  $\mathbf{T}_c \mathbf{u}_j$  ( $j = 1 \dots n$ ) are linearly independent as well. Consequently, an arbitrary vector of the relative displacements between the two terminals of the inerters  $\mathbf{x}_d$  can be expressed by a linear combination of  $\mathbf{T}_c \mathbf{u}_j$  ( $j = 1 \dots n$ ) [51]:

$$\mathbf{x}_d = \sum_{j=1}^n \xi_{d,j} \mathbf{T}_c \mathbf{u}_j \quad (45)$$

where  $\xi_{d,j}$  is the  $j$ -th modal coordinate of the inerter displacement.

From the orthogonality of the mode vectors of the undamped primary structure, if  $r \neq s$ , then it follows that

$$\mathbf{u}_r^T \mathbf{M}_p \mathbf{u}_s = 0 \quad (46)$$

$$\mathbf{u}_r^T \mathbf{K}_p \mathbf{u}_s = 0 \quad (47)$$

$$\mathbf{u}_r^T \mathbf{C}_p \mathbf{u}_s = 0 \quad (48)$$

Hence, Eqs. (33)-(35) ensure the following orthogonality relationship for SPD-TVMD if  $r \neq s$ :

$$\mathbf{u}_r^T \mathbf{T}_c^T \mathbf{M}_D \mathbf{T}_c \mathbf{u}_s = \alpha \mathbf{u}_r^T \mathbf{T}^T \mathbf{K}_0 \mathbf{T} \mathbf{u}_s = \alpha \mathbf{u}_r^T \mathbf{K}_p \mathbf{u}_s = 0 \quad (49)$$

$$\mathbf{u}_r^T \mathbf{T}_c^T \mathbf{C}_D \mathbf{T}_c \mathbf{u}_s = (2\alpha\beta^\circ h_d^\circ \omega_1) \mathbf{u}_r^T \mathbf{T}^T \mathbf{K}_0 \mathbf{T} \mathbf{u}_s = (2\alpha\beta^\circ h_d^\circ \omega_1) \mathbf{u}_r^T \mathbf{K}_p \mathbf{u}_s = 0 \quad (50)$$

$$\mathbf{u}_r^T \mathbf{T}_c^T \mathbf{K}_B \mathbf{T}_c \mathbf{u}_s = \alpha(\beta^\circ \omega_1)^2 \mathbf{u}_r^T \mathbf{T}^T \mathbf{K}_0 \mathbf{T} \mathbf{u}_s = \alpha(\beta^\circ \omega_1)^2 \mathbf{u}_r^T \mathbf{K}_p \mathbf{u}_s = 0 \quad (51)$$

Similarly, Eqs. (40)-(42) ensure the following orthogonality relationship for the MPD-TVMD if  $r \neq s$ :

$$\mathbf{u}_r^T \mathbf{T}_c^T \mathbf{M}_D \mathbf{T}_c \mathbf{u}_s = \alpha \mathbf{u}_r^T \mathbf{M}_p \mathbf{u}_s = 0 \quad (52)$$

$$\mathbf{u}_r^T \mathbf{T}_c^T \mathbf{C}_D \mathbf{T}_c \mathbf{u}_s = (2\alpha\beta^\circ h_d^\circ \omega_1) \mathbf{u}_r^T \mathbf{M}_p \mathbf{u}_s = 0 \quad (53)$$

$$\mathbf{u}_r^T \mathbf{T}_c^T \mathbf{K}_B \mathbf{T}_c \mathbf{u}_s = \alpha(\beta^\circ \omega_1)^2 \mathbf{u}_r^T \mathbf{M}_p \mathbf{u}_s = 0 \quad (54)$$

Thus, left-multiplying  $\{\mathbf{u}_k^T, \mathbf{u}_k^T \mathbf{T}_c^T\}$  to Eq. (20) and substituting Eqs. (44)-(54) yield,

$$\mathbf{M}_k \ddot{\xi}_k + \mathbf{C}_k \dot{\xi}_k + \mathbf{K}_k \xi_k = -\nu_k \mathbf{M}_k \bar{r} \ddot{x}_0 \quad (55)$$

where

$$\xi_k = \{\xi_k, \xi_{d,k}\}^T \quad (56)$$

$$\mathbf{M}_k = \begin{bmatrix} M_{p,k} & 0 \\ 0 & M_{d,k} \end{bmatrix} \quad (57)$$

$$\mathbf{C}_k = \begin{bmatrix} C_{p,k} & 0 \\ 0 & C_{d,k} \end{bmatrix} \quad (58)$$

$$\mathbf{K}_k = \begin{bmatrix} K_{p,k} + K_{b,k} & -K_{b,k} \\ -K_{b,k} & K_{b,k} \end{bmatrix} \quad (59)$$

$$\nu_k = \frac{\mathbf{u}_k^T \mathbf{M}_p \mathbf{r}}{M_{p,k}} \quad (60)$$

$$M_{p,k} = \mathbf{u}_k^T \mathbf{M}_p \mathbf{u}_k, \quad K_{p,k} = \mathbf{u}_k^T \mathbf{K}_p \mathbf{u}_k, \quad C_{p,k} = \mathbf{u}_k^T \mathbf{C}_p \mathbf{u}_k \quad (61)$$

$$M_{d,k} = \mathbf{u}_k^T \mathbf{T}_c^T \mathbf{M}_D \mathbf{T}_c \mathbf{u}_k, \quad K_{b,k} = \mathbf{u}_k^T \mathbf{T}_c^T \mathbf{K}_B \mathbf{T}_c \mathbf{u}_k, \quad C_{d,k} = \mathbf{u}_k^T \mathbf{T}_c^T \mathbf{C}_D \mathbf{T}_c \mathbf{u}_k \quad (62)$$

Note that  $M_{p,k}$ ,  $K_{p,k}$ ,  $C_{p,k}$  represent the generalized mass, stiffness, and inherent damping coefficients of the  $k$ -th mode of the primary system, respectively. Similarly,  $M_{d,k}$ ,  $K_{b,k}$ , and  $C_{d,k}$  are the generalized apparent mass, supporting spring stiffness, and damping coefficient of the secondary system (TVMDs) for the  $k$ -th mode, respectively.

Eq. (55) represents the  $k$ -th equivalent 2-DOF system reduced from Eq. (20), proving that the equations of motion of an MDOF structure controlled by SPD-TVMD and MPD-TVMD can be decomposed using the original modes of an undamped primary structure. When the target mode is the first mode, the ratio of the generalized secondary mass to the first-order generalized primary mass is

$$\mu = \frac{M_{d,1}}{M_{p,1}} = \begin{cases} \alpha\omega_1^2 & \text{SPD - TVMD} \\ \alpha & \text{MPD - TVMD} \end{cases} \quad (63)$$

Let  $\lambda_\ell^k$  and  $\lambda_\ell^{k*}$  denote the complex conjugate pair of eigenvalues, and  $\phi_\ell^k = \{\phi_\ell^k, \phi_{d,\ell}^k\}^T$ ,  $\phi_\ell^{k*} = \{\phi_\ell^{k*}, \phi_{d,\ell}^{k*}\}^T$  denote the complex conjugate pair of eigenmodes for the equivalent 2-DOF system stemming from the  $k$ -th uncontrolled system, controlled by the Eq. (55). Then,  $2n$  specific conjugate pairs of values and vectors can be constructed as follows:

$$\begin{aligned} \tilde{\lambda}_r &= \lambda_\ell^k \\ \tilde{\lambda}_r^* &= \lambda_\ell^{k*} \\ \tilde{\mathbf{u}}_r &= \begin{Bmatrix} \phi_\ell^k \mathbf{u}_k \\ \phi_{d,\ell}^k \mathbf{T}_c \mathbf{u}_k \end{Bmatrix} \\ \tilde{\mathbf{u}}_r^* &= \begin{Bmatrix} \phi_\ell^{k*} \mathbf{u}_k \\ \phi_{d,\ell}^{k*} \mathbf{T}_c \mathbf{u}_k \end{Bmatrix} \end{aligned} \quad (64)$$

where  $k = 1, 2, \dots, n$ ,  $\ell = 1, 2$ ,  $r = n(\ell - 1) + k$ .

Substituting Eqs. (28), (33)-(36), and  $\tilde{\mathbf{x}} = \tilde{\mathbf{u}}_r e^{\tilde{\lambda}_r t}$ ,  $\tilde{\mathbf{u}}_r^* e^{\tilde{\lambda}_r^* t}$  into Eq. (20) and setting  $\ddot{\mathbf{x}}_0 = 0$ , we obtain the following result for SPD-TVMD:

$$\begin{aligned} \left\{ \tilde{\lambda}_r^2 \phi_\ell^k + 2h_k \omega_k \tilde{\lambda}_r \phi_\ell^k + (1 + \eta^0) \omega_k^2 \phi_\ell^k - \eta^0 \omega_k^2 \phi_{d,\ell}^k \right\} \mathbf{u}_k^T \mathbf{M}_p \mathbf{u}_k e^{\tilde{\lambda}_r t} &= 0 \\ \left\{ \mu \tilde{\lambda}_r^2 \phi_{d,\ell}^k + 2\mu\beta^0 h_d^0 \omega_1 \tilde{\lambda}_r \phi_{d,\ell}^k - \eta^0 \omega_1^2 \phi_\ell^k + \eta^0 \omega_1^2 \phi_{d,\ell}^k \right\} \mathbf{u}_k^T \mathbf{K}_p \mathbf{u}_k e^{\tilde{\lambda}_r t} &= 0 \end{aligned} \quad (65)$$

$$\begin{aligned} \left\{ \tilde{\lambda}_r^2 \phi_\ell^{k*} + 2h_k \omega_k \tilde{\lambda}_r \phi_\ell^{k*} + (1 + \eta^0) \omega_k^2 \phi_\ell^{k*} - \eta^0 \omega_k^2 \phi_{d,\ell}^{k*} \right\} \mathbf{u}_k^T \mathbf{M}_p \mathbf{u}_k e^{\tilde{\lambda}_r^* t} &= 0 \\ \left\{ \mu \tilde{\lambda}_r^2 \phi_{d,\ell}^{k*} + 2\mu\beta^0 h_d^0 \omega_1 \tilde{\lambda}_r \phi_{d,\ell}^{k*} - \eta^0 \omega_1^2 \phi_\ell^{k*} + \eta^0 \omega_1^2 \phi_{d,\ell}^{k*} \right\} \mathbf{u}_k^T \mathbf{K}_p \mathbf{u}_k e^{\tilde{\lambda}_r^* t} &= 0 \end{aligned} \quad (66)$$

Substituting Eqs. (29), (40)-(42), and  $\tilde{\mathbf{x}} = \tilde{\mathbf{u}}_r e^{\tilde{\lambda}_r t}$ ,  $\tilde{\mathbf{u}}_r^* e^{\tilde{\lambda}_r^* t}$  into Eq. (20) and setting  $\ddot{\mathbf{x}}_0 = 0$ , we obtain the following result for MPD-TVMD:

$$\begin{aligned} \left\{ \tilde{\lambda}_r^2 \phi_\ell^k + 2h_k \omega_k \tilde{\lambda}_r \phi_\ell^k + (\omega_k^2 + \eta^0 \omega_1^2) \phi_\ell^k - \eta^0 \omega_1^2 \phi_{d,\ell}^k \right\} \mathbf{u}_k^T \mathbf{M}_p \mathbf{u}_k e^{\tilde{\lambda}_r t} &= 0 \\ \left\{ \mu \tilde{\lambda}_r^2 \phi_{d,\ell}^k + 2\mu\beta^0 h_d^0 \omega_1 \tilde{\lambda}_r \phi_{d,\ell}^k - \eta^0 \omega_1^2 \phi_\ell^k + \eta^0 \omega_1^2 \phi_{d,\ell}^k \right\} \mathbf{u}_k^T \mathbf{M}_p \mathbf{u}_k e^{\tilde{\lambda}_r t} &= 0 \end{aligned} \quad (67)$$

$$\begin{aligned} \left\{ \tilde{\lambda}_r^2 \phi_\ell^{k*} + 2h_k \omega_k \tilde{\lambda}_r \phi_\ell^{k*} + (\omega_k^2 + \eta^0 \omega_1^2) \phi_\ell^{k*} - \eta^0 \omega_1^2 \phi_{d,\ell}^{k*} \right\} \mathbf{u}_k^T \mathbf{M}_p \mathbf{u}_k e^{\tilde{\lambda}_r^* t} &= 0 \\ \left\{ \mu \tilde{\lambda}_r^2 \phi_{d,\ell}^{k*} + 2\mu\beta^0 h_d^0 \omega_1 \tilde{\lambda}_r \phi_{d,\ell}^{k*} - \eta^0 \omega_1^2 \phi_\ell^{k*} + \eta^0 \omega_1^2 \phi_{d,\ell}^{k*} \right\} \mathbf{u}_k^T \mathbf{M}_p \mathbf{u}_k e^{\tilde{\lambda}_r^* t} &= 0 \end{aligned} \quad (68)$$

where,  $\omega_k$  is the  $k$ -th angular frequency of the uncontrolled structure.

$$h_k = \frac{1}{2} \left( \alpha_k \omega_k + \frac{\alpha_M}{\omega_k} \right) \quad (69)$$

It can be observed that, since  $\mathbf{u}_k^T \mathbf{M}_p \mathbf{u}_k \neq 0$  and  $\mathbf{u}_k^T \mathbf{K}_p \mathbf{u}_k \neq 0$ , Eqs. (65)-(68) match those of the characteristic equation of the equivalent 2-DOF system controlled by the Eq. (55). According to the definitions of  $\lambda_\ell^k$ ,  $\lambda_\ell^{k*}$ , and  $\phi_\ell^k = \{\phi_\ell^k, \phi_{d,\ell}^k\}^T$ ,  $\phi_\ell^{k*} = \{\phi_\ell^{k*}, \phi_{d,\ell}^{k*}\}^T$ , it can be concluded that Eqs. (65)-(68) are always valid. Thus, the  $2n$  specific conjugate pairs of values and vectors defined by Equation (70) are indeed the eigenvalues and eigenvectors of the TVMD controlled system. By comparing the primary structure's modal vector component in the controlled structure from Equation (71) with the modal vector of the uncontrolled structure, it becomes evident that the modal vector of the primary structure remains unchanged after the installation of SPD- or MPD-TVMDs. This modal principle can be referred to as the mode-preserving characteristic.

Hence, the  $r$ -th fundamental angular frequency  $\tilde{\omega}_r$  and damping ratio  $\tilde{h}_r$  for the TVMD controlled system can be obtained as follows:

$$\tilde{\omega}_r = |\tilde{\lambda}_r| = |\tilde{\lambda}_r^*| \quad (72)$$

$$\tilde{h}_r = -\frac{\text{Re}[\tilde{\lambda}_r]}{|\tilde{\lambda}_r|} = -\frac{\text{Re}[\tilde{\lambda}_r^*]}{|\tilde{\lambda}_r^*|} \quad (73)$$

Specifically, corresponding to the target mode of the uncontrolled structure ( $k = 1, \ell = 1, 2$ ), Eqs. (65)-(68) are consistent with Eqs. (10)-(11). This indicates that the impacts of the MPD-TVMD and SPD-TVMD systems on the target modal response of MDOF structures align with their effects on a corresponding SDOF structure, including the extent to which they alter the angular frequency and increase the damping ratio.

For other modes ( $k \neq 1$ ), their eigenvalues function derived from Eqs. (65)-(68) can be approximated as follows:

$$\begin{aligned} \text{SPD-TVMD: } & \left\{ \left( \frac{\tilde{\lambda}_r}{\omega_k} \right)^2 + 2h_k \frac{\tilde{\lambda}_r}{\omega_k} + (1 + \eta^0) \right\} \left\{ \mu \left( \frac{\tilde{\lambda}_r}{\omega_k} \right)^2 + 2\mu\beta^0 h_d^0 \frac{\omega_1}{\omega_k} \left( \frac{\tilde{\lambda}_r}{\omega_k} \right) \right\} \\ & = 0 \end{aligned} \quad (74)$$

$$\text{MPD-TVMD: } \left\{ \left( \frac{\tilde{\lambda}_r}{\omega_k} \right)^2 + 2h_k \frac{\tilde{\lambda}_r}{\omega_k} + 1 \right\} \left\{ \mu \left( \frac{\tilde{\lambda}_r}{\omega_k} \right)^2 + 2\mu\beta^0 h_d^0 \frac{\omega_1}{\omega_k} \left( \frac{\tilde{\lambda}_r}{\omega_k} \right) \right\} = 0 \quad (75)$$

In this derivation, it was assumed that the natural frequencies of the structure are well-separated, i.e.,  $(\omega_1/\omega_k)^2 \rightarrow 0$ . The two sets of solutions for Eqs. (74) and (75) correspond to the eigenvalues of the uncontrolled structure and the intrinsic eigenvalues of the TVMD device, respectively. This indicates that for other modes ( $k \neq 1$ ), both SPD-TVMD and MPD-TVMD have minimal impact on their frequencies and damping coefficient of the uncontrolled structure.

The participation factors of TVMD controlled systems  $\tilde{\nu}_r$  and  $\tilde{\nu}_r^*$  can be obtained:

$$\begin{aligned} \tilde{\nu}_r &= \frac{\tilde{\mathbf{u}}_r^T \tilde{\mathbf{M}} \tilde{\mathbf{r}}}{\tilde{\mathbf{u}}_r^T \tilde{\mathbf{M}} \tilde{\mathbf{u}}_r} = \nu_\ell^k \nu_k \\ \tilde{\nu}_r^* &= \frac{\tilde{\mathbf{u}}_r^{*T} \tilde{\mathbf{M}} \tilde{\mathbf{r}}}{\tilde{\mathbf{u}}_r^{*T} \tilde{\mathbf{M}} \tilde{\mathbf{u}}_r^*} = \nu_\ell^{k*} \nu_k \end{aligned}, \quad \begin{cases} k = 1, 2, \dots, n \\ \ell = 1, 2 \\ r = n(\ell - 1) + k \end{cases} \quad (76)$$

where  $\nu_\ell^k$  and  $\nu_\ell^{k*}$  are the participation factors of the reduced 2-DOF system derived from the uncontrolled primary  $k$ -th mode are:

$$\begin{aligned} \nu_\ell^k &= \frac{\{\phi_\ell^k\}^T \mathbf{M}_k \tilde{\mathbf{r}}}{\{\phi_\ell^k\}^T \mathbf{M}_k \phi_\ell^k} \\ \nu_\ell^{k*} &= \frac{\{\phi_\ell^{k*}\}^T \mathbf{M}_k \tilde{\mathbf{r}}}{\{\phi_\ell^{k*}\}^T \mathbf{M}_k \phi_\ell^{k*}} \end{aligned} \quad (77)$$

This implies that  $\tilde{\nu}_r$  and  $\tilde{\nu}_r^*$  can be obtained by combining the participation factors of the uncontrolled primary structure  $\nu_k$  and those of the reduced 2-DOF system  $\nu_\ell^k$  and  $\nu_\ell^{k*}$ . The following relationship holds.

$$\begin{aligned} \sum_{r=1}^{2n} \left( \tilde{\nu}_r \tilde{\mathbf{u}}_r + \tilde{\nu}_r^* \tilde{\mathbf{u}}_r^* \right) &= \sum_{k=1}^n \left\{ \nu_k \sum_{\ell=1}^2 \left[ \nu_\ell^k \left\{ \begin{matrix} \phi_\ell^k \mathbf{u}_k \\ \phi_{d,\ell}^k \mathbf{T}_c \mathbf{u}_k \end{matrix} \right\} \right. \right. \\ & \quad \left. \left. + \nu_\ell^{k*} \left\{ \begin{matrix} \phi_\ell^{k*} \mathbf{u}_k \\ \phi_{d,\ell}^{k*} \mathbf{T}_c \mathbf{u}_k \end{matrix} \right\} \right] \right\} \\ &= \sum_{k=1}^n \nu_k \left\{ \begin{matrix} \mathbf{u}_k \\ 0 \end{matrix} \right\} = \tilde{\mathbf{r}} \end{aligned} \quad (78)$$

Eq. (78) shows that the uncontrolled participation mode vector  $\nu_k \mathbf{u}_k$  can be obtained by superimposing the two complex conjugate controlled mode vectors stemming from the  $k$ -th uncontrolled mode. Accordingly, the seismic responses of a TVMD controlled system can be estimated by utilizing the uncontrolled participation mode vector and added damping

coefficients without any complex-valued eigenvalue analysis of the TVMD controlled MDOF [43], which will be illustrated in Section 4.

### 4. Analytical examples

#### 4.1. 2-story shear building

In this section, a 2-story undamped shear building was employed to demonstrate the modal response characteristics of an MDOF shear building containing TVMDs. The mass of both stories in the building was 1000 kg. The stiffnesses of the first and second stories were 3000 N/m and 2000 N/m, respectively.

Fig. 3 shows the participation-mode vectors of an undamped primary system. The first and second angular frequencies of the primary system are 1.00 rad/s and 2.45 rad/s, respectively. Table 1 lists the optimum parameters for SPD-TVMD and MPD-TVMD designed based on Eqs. (5), (30)-(32), and (37)-(39). All TVMDs were tuned to the first mode with a mass ratio of  $\mu = 0.05$ . It is evident that nearly 60 % of the total apparent mass and damping coefficient requirements are saved with the use of MPD-TVMD compared to SPD-TVMD. This efficiency is attributed to the MPD-TVMD's direct utilization of the floor deformation relative to the ground, which is more effective in controlling the first mode compared to the SPD-TVMD that relies on inter-story deformation. The parameters of the two equivalent 2-DOF systems stemming from the first and second uncontrolled systems are listed in Table 2.

Table 3 summarizes the angular frequencies and damping ratios for the TVMD controlled 2-story shear building. Both SPD-TVMD and MPD-TVMD exhibited similar dynamic characteristics. As the TVMDs were tuned to the first uncontrolled mode ( $\omega = 1.00$  rad/s), the reduced 2-DOF systems derived from the uncontrolled primary modes ( $r = 1, r = 3$ ) had angular frequencies that were close to each other and to the first uncontrolled frequency ( $\omega = 1.00$  rad/s). By contrast, the first-order angular frequencies of the reduced 2-DOF systems derived from the uncontrolled second mode ( $r = 2$ ) were closer to the first uncontrolled frequency ( $\omega = 1.00$  rad/s) than to the second uncontrolled frequency ( $\omega = 2.45$  rad/s). Moreover, the second angular frequencies of the reduced 2-DOF systems derived from the uncontrolled second mode ( $r = 4$ ) were close to the second uncontrolled angular frequency ( $\omega = 2.45$  rad/s).

The first participation mode vectors of the reduced 2-DOF systems ( $\ell = 1$ ) are shown in the left half of Figs. 4(a) and 5(a), whereas the second mode vectors ( $\ell = 2$ ) are shown on the right-hand side. Therefore, according to Eqs. (64) and (76), combined with the participation mode vectors of the undamped primary system shown in Fig. 3, the complex-valued participation vectors of the entire TVMD controlled system can be obtained, as depicted in Fig. 4(b) and 5 (b). For comparison, the complex-valued participation vectors obtained by directly solving the complex modal equation of the controlled system are also marked in Fig. 4(b) and 5 (b) using blue hollow circles. The overlap between the

**Table 1**

Optimum parameters for the distributed TVMDs.

story	Stiffness proportionally			Mass proportionally		
	$m_d$ [kg]	$k_b$ [N/m]	$c_d$ [N-s/m]	$m_d$ [kg]	$k_b$ [N/m]	$c_d$ [N-s/m]
1	150.00	167.18	44.56	50.00	55.73	14.85
2	100.00	111.46	29.70	50.00	55.73	14.85

**Table 2**

Specifications for the reduced 2-DOF systems.

$k$	Cases	$M_{d,k}$ [kg]	$K_{d,k}$ [N/m]	$C_{d,k}$ [N-s/m]	$\mu_k$	$h_{d,k}$	$\eta_k$
1	SPD	90.00	100.31	26.74	0.050	0.141	0.056
2		60.00	66.87	17.82	0.300	0.141	0.056
1	MPD	90.00	100.31	26.74	0.050	0.141	0.056
2		10.00	11.15	2.97	0.050	0.141	0.009

blue hollow circles and the red dots numerically validates the accuracy of the participation mode vectors constructed in Eqs. (64) and (76).

Evidently, the complex-valued participation vectors for the first and third modes ( $r = 1$  and 3) in Fig. 4(b) and 5 (b) demonstrate that adding TVMD splits the uncontrolled first mode ( $k = 1$ ) into two coupled modes ( $r = 1$ ) and ( $r = 3$ ), which have similar natural angular frequencies of 0.936 rad/s and 1.128 rad/s, respectively. The motion of the inerter was enhanced by the tuning effect. Because the TVMD is detuned when incorporated into the 2-DOF system stemming from the second mode ( $k = 2$ ) of the uncontrolled system, the complex-valued participation vectors for the second and fourth modes ( $r = 2$  and  $r = 4$ ) in Fig. 4(b) and 5 (b) show that adding TVMD splits the uncontrolled second mode into two decoupled modes ( $r = 2$ ) and ( $r = 4$ ) with natural angular frequencies of 1.022 rad/s and 2.531 rad/s, or 1.050 rad/s and 2.463 rad/s. The motion of TVMD dominates the second mode of the controlled system ( $\ell = 1$  and  $k=2$ ), whereas the controlled fourth mode ( $\ell = 2$  and  $k=2$ ) is dominated by the uncontrolled second mode.

The damping ratios of the TVMD controlled 2-story shear building are listed in Table 3. For both SPD-TVMD and MPD-TVMD, the damping ratios of the first and second modes of the reduced 2-DOF systems stemming from the first uncontrolled mode ( $\ell = 1, 2$  and  $k = 1$ ) were identical to the value when  $h = 0.072$ . This is consistent with the optimal

**Table 3**

Angular frequencies and damping ratios for the TVMD controlled 2-story shear building.

$\ell$	$k$	$r$	SPD-TVMD		MPD-TVMD	
			$\tilde{\omega}_r$ [rad/s]	$\tilde{h}_r$	$\tilde{\omega}_r$ [rad/s]	$\tilde{h}_r$
1	1	1	0.936	0.072	0.936	0.072
	2	2	1.022	0.144	1.050	0.141
2	1	3	1.128	0.072	1.128	0.072
	2	4	2.531	0.001	2.463	0.001

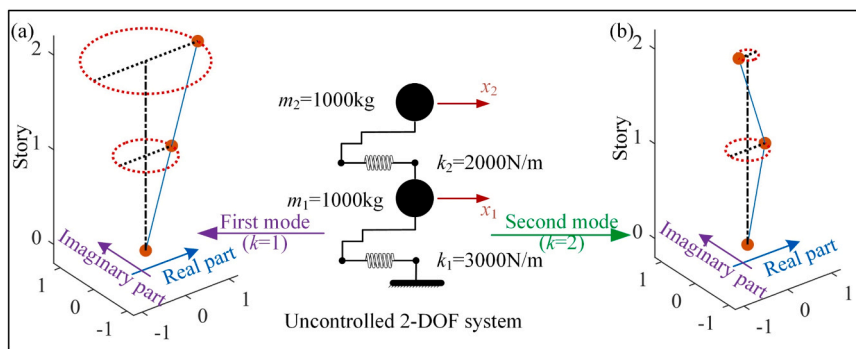


**Fig. 3.** Participation-mode vectors of an undamped 2-story shear building without considering the inherent damping ratio: (a) First mode ( $k = 1$ ). (b) Second mode ( $k = 2$ ).

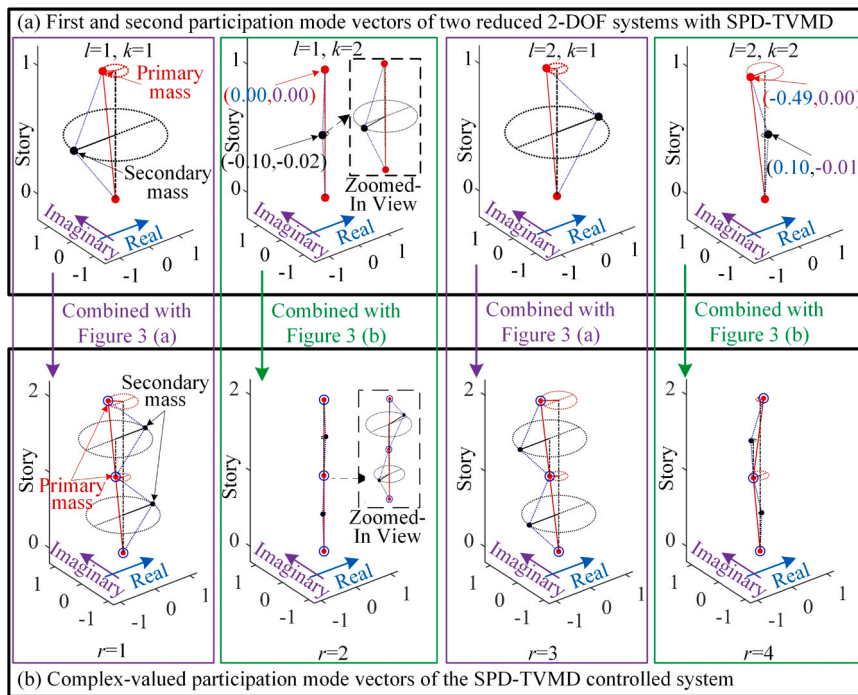


Fig. 4. Modal principle of SPD-TVMD illustrated by a 2-story shear building: (a) First and second participation mode vectors ( $\ell = 1, 2$ ) of two reduced 2-DOF systems with SPD-TVMD ( $k = 1, 2$ ). (b) Comparison between the complex-valued participation vectors of the SPD-TVMD controlled system obtained by combining methods and complex modal analysis.

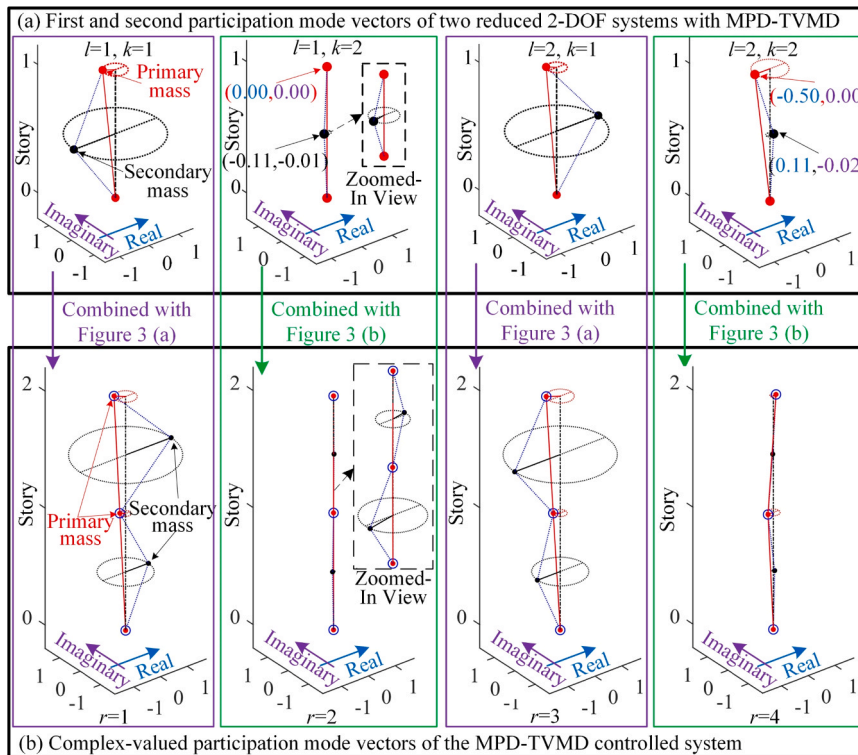


Fig. 5. Modal principle of MPD-TVMD illustrated by a 2-story shear building: (a) First and second participation mode vectors ( $\ell = 1, 2$ ) of two reduced 2-DOF systems with MPD-TVMD ( $k = 1, 2$ ). (b) Comparison between the complex-valued participation vectors of the MPD-TVMD controlled system obtained by combining methods and complex modal analysis.

condition for the transfer function of a TVMD controlled SDOF system to have the same peak value. The first-mode damping ratios of the reduced 2-DOF systems stemming from the second uncontrolled mode for the

SPD-TVMD and MPD-TVMD ( $\ell = 1$  and  $k = 2$ ) were 0.144 and 0.141, respectively, which were close to the damping ratio of the TVMDs ( $h_d=0.141$ ). Notably, according to the corresponding complex-valued

participation vectors for  $\ell = 1$  and  $k = 2$  shown in Fig. 4(b) and 5 (b), it can be observed that the motion of the TVMDs dominated, and the primary mass was barely activated; thus, the participation of this mode in the seismic response was negligible. In contrast, as the fourth complex-valued participation vectors in Fig. 4(b) and 5 (b) show, the TVMDs were barely activated in the second mode of the reduced 2-DOF system stemming from the second uncontrolled mode ( $\ell = 2$  and  $k = 2$ ); thus, their damping ratios were very small. This means that TVMDs are activated only by the target mode, and thereby perform selective damping for the target mode.

As a representation of the harmonic response, Fig. 6 compares the displacement amplification factor curves of the uncontrolled, SPD-TVMD-controlled, and MPD-TVMD-controlled 2-story shear building. It can be observed that the damping effects of SPD-TVMD and MPD-TVMD are similar. After the installation of proportionally distributed TVMDs, the displacement amplification factor curves for each story exhibit similar peak values near the target control mode frequency ( $\omega = 1.00$  rad/s), consistent with the effects observed in SDOF structure shown in Fig. 1(b). For another mode ( $\omega = 2.45$  rad/s), the displacement amplification factor curves of the proportionally distributed TVMDs are similar to those of the uncontrolled structure, which is consistent with the theoretical analysis results in Section 3.2.

#### 4.2. 10-story benchmark steel building

In this section, a 10-story benchmark building model [52] was employed to examine the effect of the TVMD distribution on the mode shapes considering some practical issues. Table 4 lists the specifications of the 10-story building. The primary structure was assumed to remain elastic and possess an inherent damping ratio of 0.02 for the first mode. Fig. 7 shows the mode shapes and modal interstory drifts of the participation mode of an uncontrolled primary structure. The first two fundamental angular frequencies are shown in Fig. 7 as well.

##### 4.2.1. 10-story benchmark steel building containing SPD-TVMD

With a mass ratio  $\mu = 0.1$ , the optimal frequency ratio  $\beta^o$  and supplemental damping ratio  $h_d^o$  were determined to be 1.127 and 0.206, respectively. Table 5 lists the specifications of SPD-TVMD obtained using Eqs. (30)-(32). This TVMD distribution pattern is hereafter referred to as Case A. Because the number of dampers usually varies in a discrete manner in practical structural design, another more realistic case in which the TVMDs are distributed in a discrete manner is considered, hereafter referred to as Case B. Fig. 8(a) depicts the apparent mass distributions of Cases A and B. As shown in Fig. 8(b), in Case B, each TVMD device has an apparent mass of 1000 t, which can be achieved using the mass amplification effect produced by a ball-screw mechanism [1,2]. The maximum deviation in the apparent mass between Cases A and B was 22.98 %.

Fig. 9(a) depicts the two pairs of conjugate participation mode

**Table 4**  
Specification of the analytical model.

story	primary structure		
	mass $m_i$ [t]	stiffness $k_i$ [kN/m]	height [m]
10	875.41	158550.00	4.00
9	649.49	180110.00	4.00
8	656.22	220250.00	4.00
7	660.20	244790.00	4.00
6	667.24	291890.00	4.00
5	670.10	306160.00	4.00
4	675.71	328260.00	4.00
3	680.00	383020.00	4.00
2	681.63	383550.00	4.00
1	699.90	279960.00	6.00

vectors  $v_1^k \phi_\ell^k$  and  $v_1^{k*} \phi_\ell^{k*}$  ( $\ell = 1, 2$ ) of equivalent 2-DOF systems stemming from the first two uncontrolled modes ( $k = 1$  and 2). The primary system displacement relative to the ground  $\phi_\ell^k$ , inerter's relative displacement  $\phi_{d,\ell}^k$ , and deformation of the supporting spring ( $\phi_\ell^k - \phi_{d,\ell}^k$ ) are represented by  $\circ$ ,  $*$ , and  $\triangle$ , respectively. Notably, each value shown in this figure is doubled, considering the value of its conjugate mode. The figure shows that the relative displacements of the inerter and supporting spring are significantly larger than the relative displacement of the primary mass, and their phases oppose each other in the target mode ( $k = 1$ ). It means that well-designed TVMD will resonate with the primary structure at the target control mode ( $k = 1$ ), effectively amplifying the displacement of the damping element in parallel with the inerter.

Fig. 9(b) and (e) compare the primary structure and supporting spring displacement participation mode vectors of the SPD-TVMD controlled system obtained by two different methods: one method involves constructing the participation mode vectors as outlined in Eqs. (64) and (76), while the other method uses complex-valued eigenvalue analysis directly without modal decomposition. The results obtained by the former method are hereafter referred to as SPD-Baseline and are indicated by solid lines. In the figure, Case A, shown by hollow circles, represents the result obtained using the complex-valued eigenvalue analysis directly, while the participation mode vectors of Case B are indicated by solid circles. The red and blue lines represent the real and imaginary parts, respectively. The complex-valued eigenvalue analysis result of Case A is consistent with that of SPD-Baseline, numerically reaffirming the mode-preserving characteristic of the proportionally distributed TVMD controlled system discussed in Section 3.

Although the participation mode vectors of Case B differ slightly from those of Case A, owing to the difference in apparent mass distribution, as shown in Fig. 9(b), the differences in the modes that dominate the seismic response are practically negligible. More specifically, the differences in the rooftop displacements of the participation mode

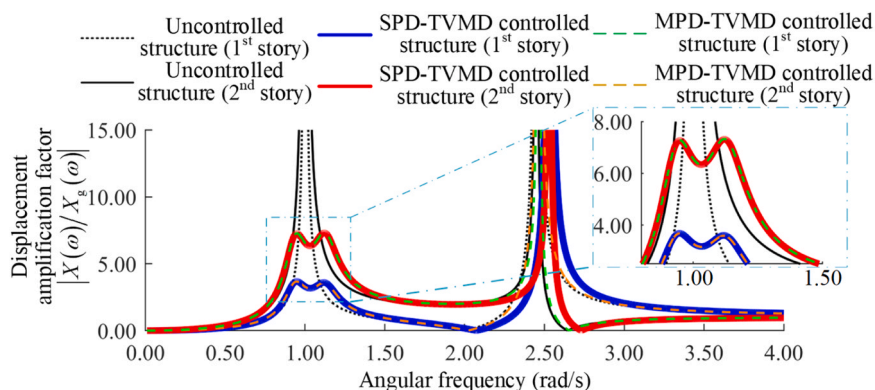


**Fig. 6.** Displacement amplification factor curves of the uncontrolled, SPD-TVMD-controlled, and MPD-TVMD-controlled 2-story shear buildings.

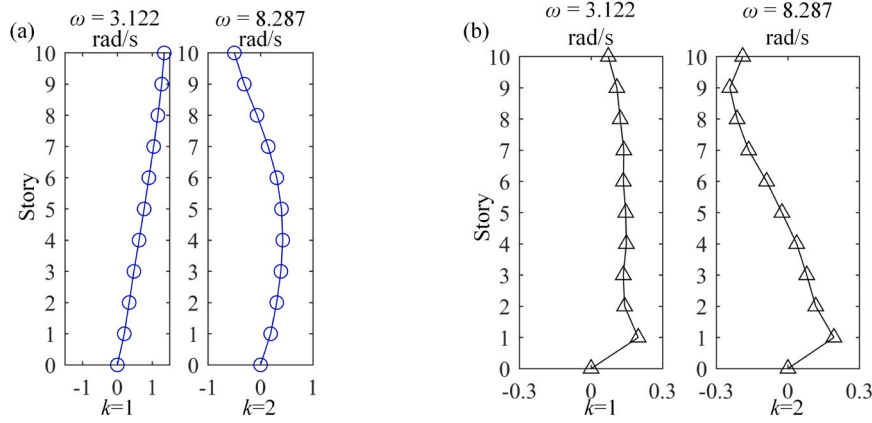


Fig. 7. Participation mode vectors of the uncontrolled primary system. (a) Displacement relative to ground. (b) Inter-story drifts.

Table 5  
Specification of SPD-TVMD.

story (i)	SPD-TVMD ( Case A)		
	$m_{d,i}$ [t]	$c_{d,i}$ [kN-s/m]	$k_{b,i}$ [kN/m]
10	1626.22	2352.96	20138.49
9	1847.36	2672.92	22876.97
8	2259.07	3268.61	27975.42
7	2510.77	3632.80	31092.41
6	2993.87	4331.79	37074.89
5	3140.23	4543.56	38887.42
4	3366.91	4871.53	41694.49
3	3928.57	5684.20	48649.92
2	3934.01	5692.06	48717.24
1	2871.50	4154.74	35559.58

vectors that stem from the undamped first mode ( $k = 1$ ) between Cases A and B were 0.9 % and 1.42 %, respectively. This implies that the mode-preserving characteristic is precisely maintained when the TVMD strictly follows the SPD pattern. However, even when the SPD pattern is only approximately followed due to practical engineering considerations, as in Case B, the modes of the uncontrolled structure can still be approximately preserved.

As shown in Fig. 9(c), the phase angles of the first ( $r = 1$ ) and eleventh modes ( $r = 11$ ) of Case A are  $30.9^\circ$  and  $-39.1^\circ$ , respectively, which stem from the first equivalent 2-DOF system as shown in Fig. 6(a) ( $k = 1$ ). In contrast, the corresponding phase angles in Case B were  $31.0^\circ$

and  $-39.3^\circ$ . This indicates that the improvement in first-mode damping for both Case A and Case B is nearly consistent with the enhancement in modal damping that the TVMD achieves in the SDOF system.

#### 4.2.2. 10-story benchmark steel building containing MPD-TVMD

Although implementing a mass proportional distribution pattern in practical is often challenging due to the requirements for floor-to-ground device installations, the superior device utilization efficiency offered by this pattern compared to stiffness proportional distribution pattern is notably promising [46–48]. This section proposes a lightweight, flexible external braced frame for implementing the MPD-TVMD system and verifies the impact of the external braced frame’s flexibility and mass on its mode-preserving characteristic. As shown in the planar and transverse sections (Y direction) in Fig. 10, two external frames are symmetrically distributed on both sides of the structure and are connected to the main structure via TVMDs.

Assuming the floors are rigid in the horizontal plane and the masses are concentrated at the floor levels, due to the symmetry of the frames, we can equivalently represent the two external frames as a single external frame in the mathematical expressions. Let  $\mathbf{M}_{exo}$  and  $\mathbf{K}_{exo}$  represent the equivalent mass and stiffness matrices of the external braced frame, respectively; the motion equations of the 10-story benchmark steel building connected with external braced frames via the MPD-TVMD system subjected to strong ground motion can be expressed as:

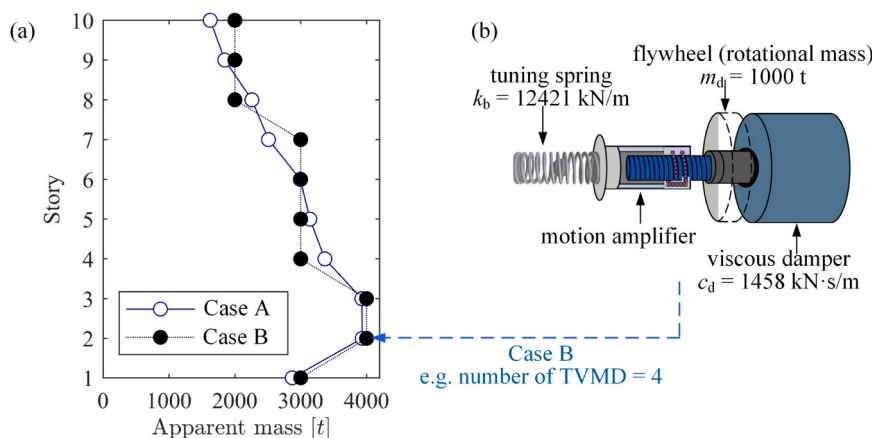
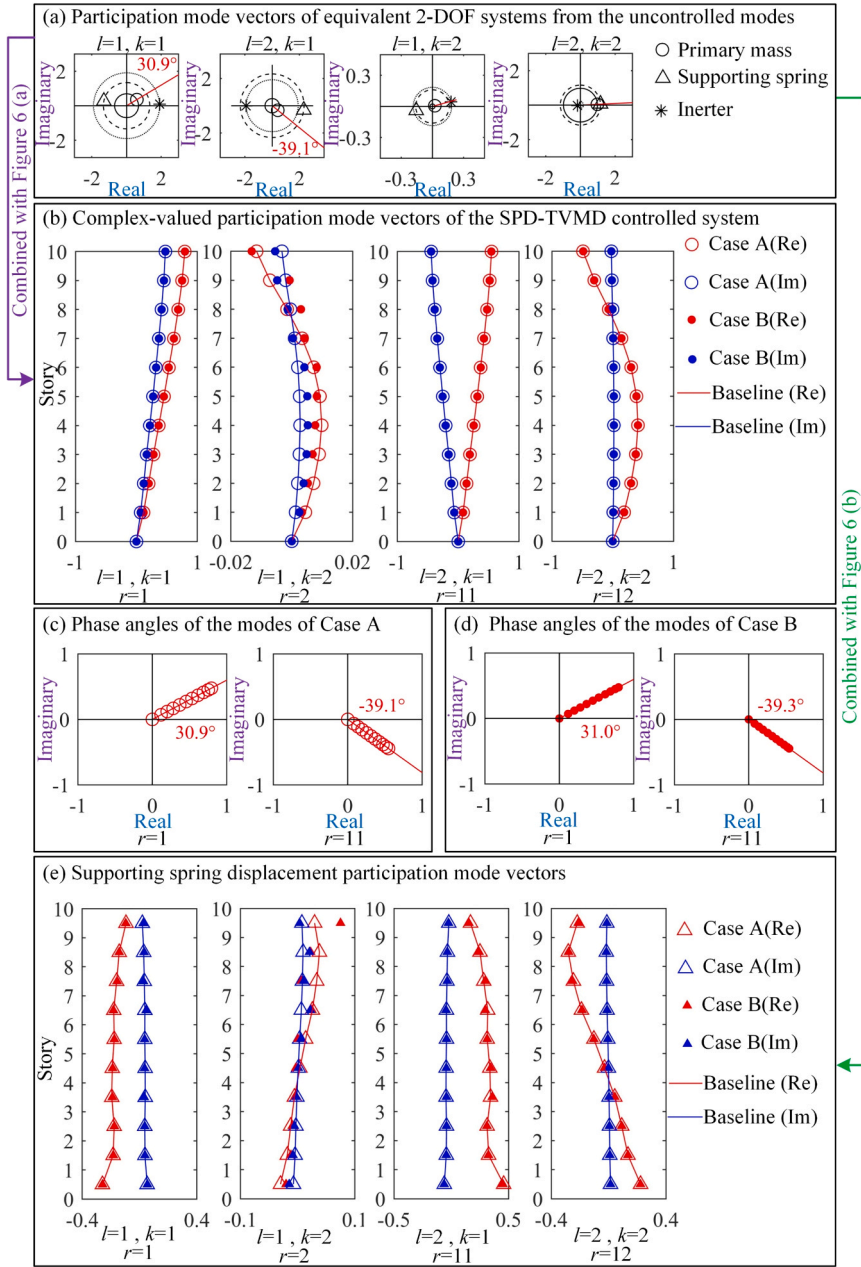


Fig. 8. Apparent mass distributions for SPD-TVMDs: (a) Ideal apparent mass distribution (Case A) and practical apparent mass distribution (Case B). (b) TVMD device in Case B with 1000 t apparent mass achieved through a ball-screw mechanism.



**Fig. 9.** Modal principle of the SPD-TVMD controlled 10-DOF system: (a) Conjugate participation mode vectors ( $\ell = 1, 2$ ) of equivalent 2-DOF systems from the first two uncontrolled modes ( $k = 1, 2$ ). (b) Comparison of participation mode vectors of the SPD-TVMD controlled system obtained by modal decomposition (Eqs. (64) and (76)) and by direct complex-valued eigenvalue analysis. (c) Phase angles of the first ( $r = 1$ ) and eleventh ( $r = 11$ ) modes of Case A. (d) Phase angles of the first ( $r = 1$ ) and eleventh ( $r = 11$ ) modes of Case B. (e) Supporting-spring displacement modes comparison for the Baseline and Cases A and B.

$$\begin{bmatrix} \mathbf{M}_p & \mathbf{0} & \mathbf{0} \\ \mathbf{0} & \mathbf{M}_D & \mathbf{0} \\ \mathbf{0} & \mathbf{0} & \mathbf{M}_{exo} \end{bmatrix} \begin{Bmatrix} \ddot{\mathbf{x}} \\ \ddot{\mathbf{x}}_d \\ \ddot{\mathbf{y}} \end{Bmatrix} + \begin{bmatrix} \mathbf{C}_p & \mathbf{0} & \mathbf{0} \\ \mathbf{0} & \mathbf{C}_D & \mathbf{0} \\ \mathbf{0} & \mathbf{0} & \mathbf{0} \end{bmatrix} \begin{Bmatrix} \dot{\mathbf{x}} \\ \dot{\mathbf{x}}_d \\ \dot{\mathbf{y}} \end{Bmatrix} + \begin{bmatrix} \mathbf{K}_p + \mathbf{K}_B & -\mathbf{K}_B & -\mathbf{K}_B \\ -\mathbf{K}_B & \mathbf{K}_B & \mathbf{K}_B \\ -\mathbf{K}_B & \mathbf{K}_B & \mathbf{K}_{exo} + \mathbf{K}_B \end{bmatrix} \begin{Bmatrix} \mathbf{x} \\ \mathbf{x}_d \\ \mathbf{y} \end{Bmatrix} = - \begin{Bmatrix} \mathbf{M}_p \mathbf{r} \\ \mathbf{0} \\ \mathbf{M}_{exo} \mathbf{r} \end{Bmatrix} \ddot{\mathbf{x}}_0 \quad (79)$$

where  $\mathbf{y} = \{y_1, y_2, \dots, y_{10}\}^T$  is the displacement vector of the external braced frame and the stiffness matrix for the supporting springs  $\mathbf{K}_B$  is a diagonal matrix.

$$\mathbf{K}_B = \mu (\beta_1^\omega)^2 \text{diag}(m_1, m_2, \dots, m_{10}) \quad (\cdot: \text{Equations(39)and(41)}) \quad (80)$$

Since the lightweight external braced frame is primarily introduced to provide support for the TVMDs, the weight of the external braced frame can be ignored ( $\mathbf{M}_{exo} = \mathbf{0}$ ), Eq. (79) can be simplified using static condensation.

$$\begin{bmatrix} \mathbf{M}_p & \mathbf{0} \\ \mathbf{0} & \mathbf{M}_D \end{bmatrix} \begin{Bmatrix} \ddot{\mathbf{x}} \\ \ddot{\mathbf{x}}_d \end{Bmatrix} + \begin{bmatrix} \mathbf{C}_p & \mathbf{0} \\ \mathbf{0} & \mathbf{C}_D \end{bmatrix} \begin{Bmatrix} \dot{\mathbf{x}} \\ \dot{\mathbf{x}}_d \end{Bmatrix} + \begin{bmatrix} \mathbf{K}_p + \mathbf{K}_B - \mathbf{K}'_{exo} & -\mathbf{K}_B + \mathbf{K}'_{exo} \\ -\mathbf{K}_B + \mathbf{K}'_{exo} & \mathbf{K}_B - \mathbf{K}'_{exo} \end{bmatrix} \begin{Bmatrix} \mathbf{x} \\ \mathbf{x}_d \end{Bmatrix} = - \begin{Bmatrix} \mathbf{M}_p \mathbf{r} \ddot{\mathbf{x}}_0 \\ \mathbf{0} \end{Bmatrix} \quad (81)$$

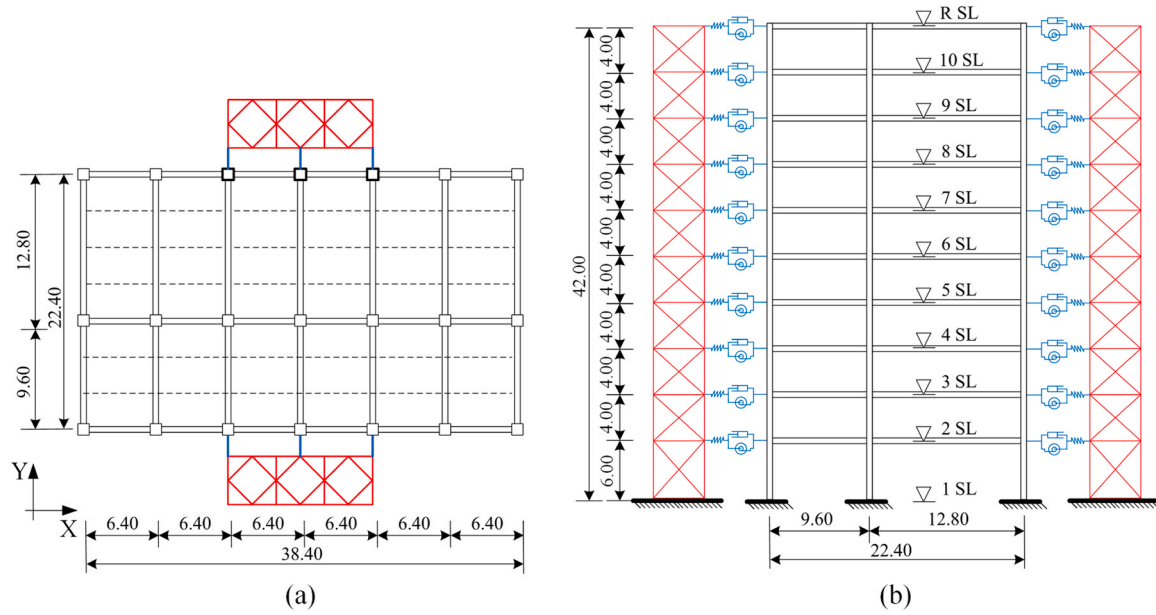


Fig. 10. 10-story benchmark steel building with the MPD-TVMD based external dissipative system: (a) Planar view showing the layout of the building with the positions of the MPD-TVMD devices. (b) Elevation view illustrating the placement of MPD-TVMD devices on each story along with the supporting structural elements.

where

$$\mathbf{K}'_{\text{exo}} = \mathbf{K}_B (\mathbf{K}_{\text{exo}} + \mathbf{K}_B)^{-1} \mathbf{K}_B \quad (82)$$

By replacing the stiffness matrix for optimal supporting spring  $\mathbf{K}_B$  in  $\tilde{\mathbf{K}}$  of Eq. (21) with  $\mathbf{K}_B - \mathbf{K}'_{\text{exo}}$ , we get Eq. (81), which results in detuning of the MPD-TVMD system. Notably, when the external braced frames are sufficiently rigid, their displacements are negligible, resulting in  $\mathbf{K}'_{\text{exo}} \approx \mathbf{O}$ . Then, Eq. (81) reduces to Eq. (20).

Here, we consider a set of supporting spring stiffnesses  $k'_{d,j}$  and define the relevant stiffness matrices as follows:

$$\mathbf{K}'_B = \text{diag}(k'_{b,1}, k'_{b,2}, \dots, k'_{b,10}) \quad (83)$$

$$\mathbf{K}''_{\text{exo}} = \mathbf{K}'_B (\mathbf{K}_{\text{exo}} + \mathbf{K}'_B)^{-1} \mathbf{K}'_B \quad (84)$$

The detuning effect induced by the flexibility of the external braced

frame can be improved by redesigning the supporting spring stiffnesses  $k'_{d,j}$  such that

$$\{k'_{d,j}\} = \left\{ \left\{ k'_{d,j} \right\} \left| \min_{k'_{d,j}} \left| \mathbf{K}_B - \mathbf{K}'_B + \mathbf{K}''_{\text{exo}} \right| \right. \right\} \quad (85)$$

Here, the results obtained by the modal decomposition method and direct eigenvalue analysis of the controlled structure for the MPD-TVMD system are referred to as MPD-Baseline and Case C, respectively. In Cases D and E, the flexibility of the external braced frame was considered. Notably, unlike the requirement in the study of MPD viscous dampers by Trombetti *et al.* [46–48], which necessitates significantly higher stiffness in external braced frame, often several times that of the primary structure to prevent displacement loss, the external braced frame in MPD-TVMD can function as part of the tuning spring. Consequently, its stiffness only needs to be slightly higher than or equal to the optimal tuning stiffness required by the TVMD at that story, making the supporting spring stiffnesses in Eq. (82) physically realizable. In this

Table 6  
Specification of MPD-TVMD.

story	Case C			Cases D and E		
	$m_{d,i}$ [t]	$c_{d,i}$ [kN-s/m]	$k_{b,i}$ [kN/m]	$m_{d,i}$ [t]	$c_{d,i}$ [kN-s/m]	$k_{b,i}$ [kN/m]
10	87.54	126.66	1084.07		100.36	863.66 (985.08)
9	64.95	93.97	804.30	70.00	100.36	863.66 (986.49)
8	65.62	94.95	812.64	70.00	100.36	863.66 (987.12)
7	66.02	95.52	817.57	70.00	100.36	863.66 (987.99)
6	66.72	96.54	826.29	70.00	100.36	863.66 (988.36)
5	67.01	96.96	29.83	70.00	100.36	863.66 (988.60)
4	67.57	97.77	836.78	70.00	100.36	863.66 (988.76)
3	68.00	98.39	842.09	70.00	100.36	863.66 (988.85)
2	68.16	98.62	844.11	70.00	100.36	863.66 (988.90)
1	69.99	101.27	866.73	70.00	100.36	863.66 (988.90)

context, we assume that  $K_{exo} = K_p$ .

Table 6 lists the specifications of MPD-TVMD obtained from Eqs. (37)-(39) (MPD-Baseline and Case C), assuming a mass ratio of  $\mu = 0.1$  and a rigid external braced frame. Because changing the properties of the device story-by-story, such as in Case C, is unrealistic, TVMDs with an apparent mass of 70.00 t are incorporated at each floor level in Cases D and E. In Case D, the supporting spring stiffnesses is determined by Eq. (39), whereas it is determined by Eq. (85) in Case E. As a result, the TVMDs in Case D are detuned, whereas they are well-tuned in Case E.

The redesigned supporting spring stiffness obtained from Eq. (85) for Case E is indicated in parenthesis in Table 6. A comparison of the total apparent mass and damping coefficient requirements between Cases D and E with the parameters of Case B, which represents the realistic distribution patterns of SPD-TVMD, reveals that the total apparent mass and damping coefficient requirements are reduced by more than 90 % with MPD-TVMD compared to SPD-TVMD. This indicates that the MPD pattern is highly efficient in utilizing TVMDs, although it comes at the cost of requiring additional structural components, such as external

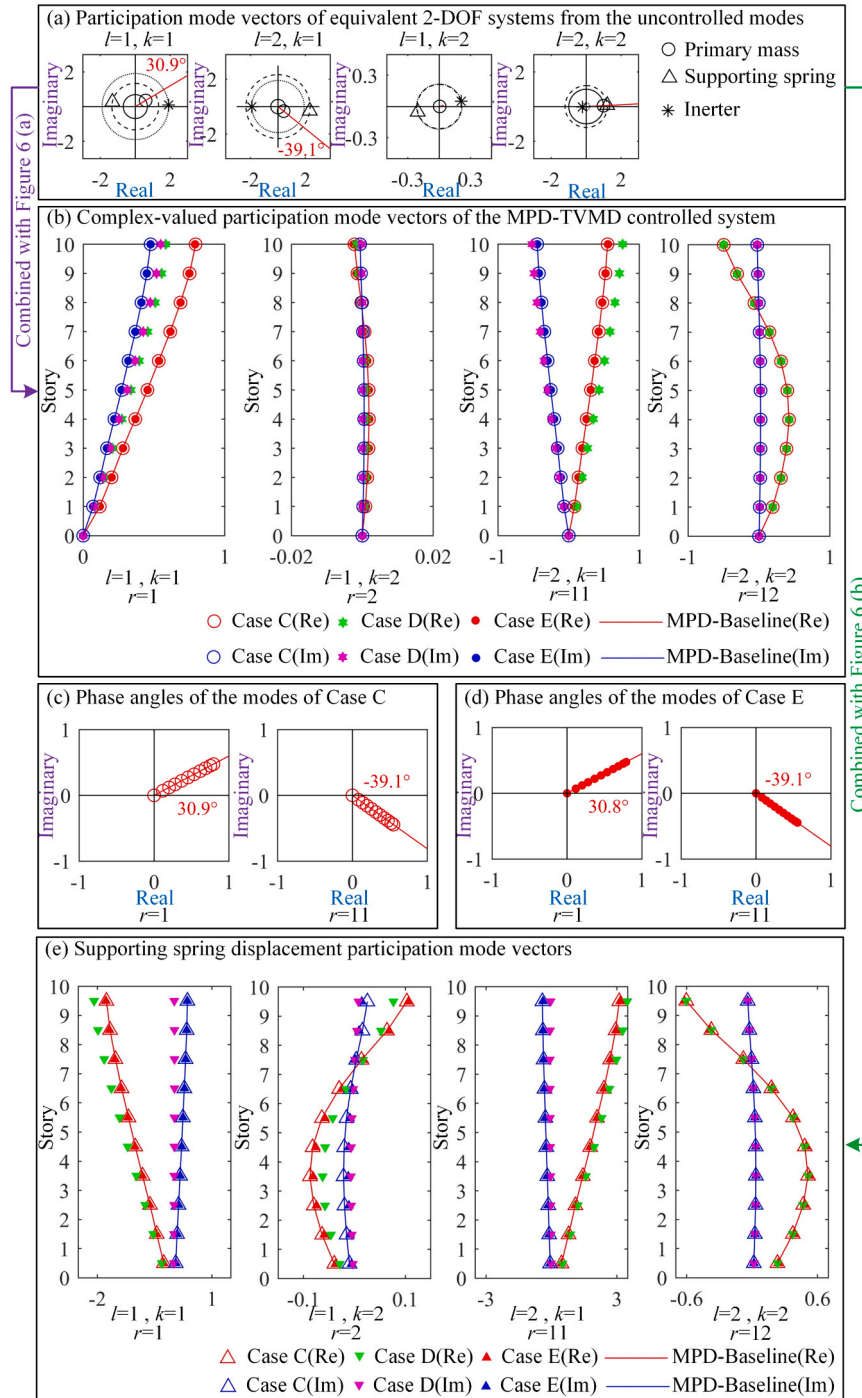


Fig. 11. Modal principle of the MPD-TVMD controlled 10-DOF system: (a) Conjugate participation mode vectors ( $\ell = 1, 2$ ) of equivalent 2-DOF systems from the first two uncontrolled modes ( $k = 1, 2$ ). (b) Comparison of participation mode vectors of the MPD-TVMD controlled system obtained by modal decomposition (Eqs. (64) and (76)) and by direct complex-valued eigenvalue analysis, showing the deviation caused by the flexibility of external braced frame. (c) Phase angles of the first ( $r = 1$ ) and eleventh ( $r = 11$ ) modes of Case C. (d) Phase angles of the first ( $r = 1$ ) and eleventh ( $r = 11$ ) modes of Case E. (e) Supporting-spring displacement mode vectors comparison for the Baseline and Cases C, D, and E.

braced frames.

Fig. 11 (a) depicts the participation mode vectors of the equivalent 2-DOF systems of the MPD-TVMD controlled system. Similar to those of the SPD-TVMD, the relative displacements of the inerter and supporting spring were significantly larger than the displacement of the primary mass, and their phases opposed each other in the target mode ( $k = 1$ ), thereby demonstrating the damping enhancement effect of TVMD. Moreover, Fig. 11 (b) and (e) depicts the participation mode vectors and supporting spring deformation in Case D, where the displacements of the primary masses and supporting springs are  $\circ$  and  $\triangle$ , respectively. Evidently, the participation mode vectors of Case D deviate from MPD-Baseline and Case C. The primary cause is the flexibility of the external braced frame. The participation mode vectors depicted in Fig. 11 (b)–(e) for Cases C and E are consistent with the MPD-Baseline. This confirmed that modifying the tuning spring’s stiffness to cancel the flexibility of the external braced frame improved the tuning effect, even when the external braced frame was as flexible as the primary structure.

Fig. 12 illustrates the impact of the external braced frame’s mass on the mode-preserving characteristic of the MPD-TVMD. In this analysis, the stiffness parameters of the external braced frame and the design parameters of the MPD-TVMD are consistent with those in Case E, while the mass of each story of the external braced frame is proportional to the mass of the corresponding story in the benchmark building, with the proportionality factor denoted as  $\mu_E$ , i.e.,  $M_{exo} = \mu_E M_p$ . In Fig. 12(a), scatter points in different colors represent the two controlled modes that split from the first uncontrolled mode due to the installation of the MPD-TVMD under various values of  $\mu_E$ . A comparison with the ideal condition (Baseline) shows that as the mass ratio increases, the controlled modes progressively deviate from the Baseline. As shown in Fig. 12 (b), this deviation is quantified based on the maximum differences in the rooftop displacements of the participation mode vectors between the MPD-TVMD systems with varying  $\mu_E$ . It indicates that when the mass of the external braced frame is kept at a relatively low level, for instance, less than 5.2 % of the mass of the benchmark building, this deviation remains minimal.

#### 4.2.3. Comparison of dynamic responses

First, from the perspective of harmonic response, Fig. 13 compares the displacement amplification factor curves for the 5th and 10th stories of the 10-story benchmark steel building without control, and with practical SPD-TVMD (Case B) and practical MPD-TVMD (Case E). As a supplement, the displacement amplification factor curves for all stories of the relevant systems are presented in Appendix A, Figures A.1 to A.3. It can be observed that the damping effects of practical SPD-TVMD and MPD-TVMD are similar, both significantly reducing the peak response

near the first mode ( $\omega = 3.122$ ).

Consequently, based on the aforementioned discussion, it can be concluded that the TVMDs installed according to the proportional distribution pattern proposed in this study, namely SPD-TVMD and MPD-TVMD, offer the advantage of enhancing the damping ratio of a specific mode without affecting the other modal characteristics. As a result, engineers can quickly estimate TVMD controlled structures using methods such as the Square Root of the Sum of Squares (SRSS) method [50].

Consider the example of a 10-story building controlled by SPD-TVMD (Cases A and B) and MPD-TVMD (Cases C and E), with the target control mode being the first mode. As depicted in Fig. 1(c), after the installation of TVMDs with a mass ratio  $\mu = 0.1$ , the first mode damping of the controlled structure increases from 0.02 to 0.114. Based on this, the peak displacement responses of the controlled and uncontrolled structures can be rapidly estimated using the SRSS method as follows:

$$x_{un,i} = \sqrt{(S_d(\omega_1, 0.02)\nu_1 u_{1,i})^2 + \sum_{k=2}^{10} (S_d(\omega_k, h_k)\nu_k u_{k,i})^2} \quad i = 1 \dots 10 \tag{86}$$

$$x_{con,i} = \sqrt{(S_d(\omega_1, 0.114)\nu_1 u_{1,i})^2 + \sum_{k=2}^{10} (S_d(\omega_k, h_k)\nu_k u_{k,i})^2} \quad i = 1 \dots 10 \tag{87}$$

where,  $x_{un,i}$  and  $x_{con,i}$  correspond to the displacements of the  $i$ -th story for the uncontrolled and controlled structures, respectively.  $u_{k,i}$  represents the  $i$ -th component of the  $k$ -th mode vector of the uncontrolled structure.  $S_d(\omega_k, h_k)$  represents the spectral displacement response of a SDOF system with a damping ratio of  $h_k$  and a frequency of  $\omega_k$ . As an illustration, an artificial earthquake wave was generated using the earthquake signal-processing tool EQSignal [53], targeting the design spectrum from the Code for Seismic Design of Buildings of China (site classification: IV) [54]. The spectral displacement response of an artificial earthquake wave considering damping ratios of 0.02, 0.053 (the first and second mode damping of the uncontrolled structure), and 0.114 (the first mode damping of the controlled structure) are presented in Fig. 14 (a).

It is noteworthy that the modal information required for the above calculation involves only the uncontrolled structure, which is familiar to designers. The only difference in response calculation between the uncontrolled and controlled structures lies in the use of different first mode

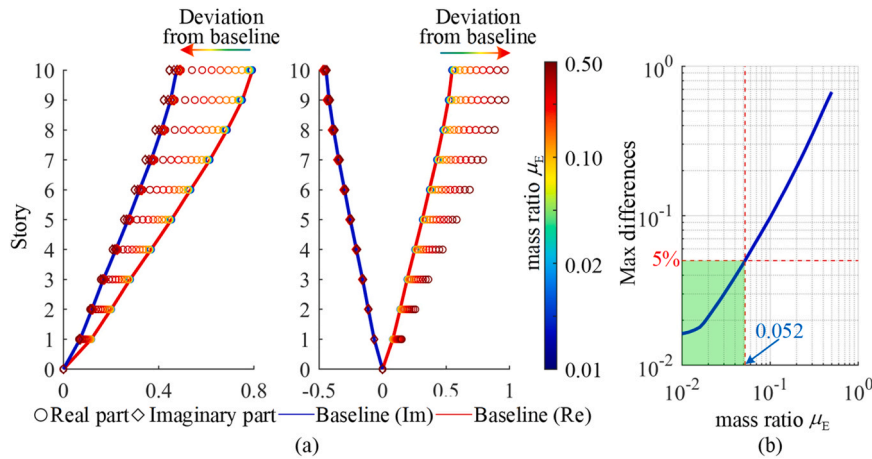


Fig. 12. The impact of the external braced frame’s mass on the mode-preserving characteristic of the MPD-TVMD system: (a) Participation mode vectors of the MPD-TVMD controlled systems corresponding to the first uncontrolled mode. (b) The relationship between the deviation of the controlled mode from the baseline and the mass of the external braced frame.

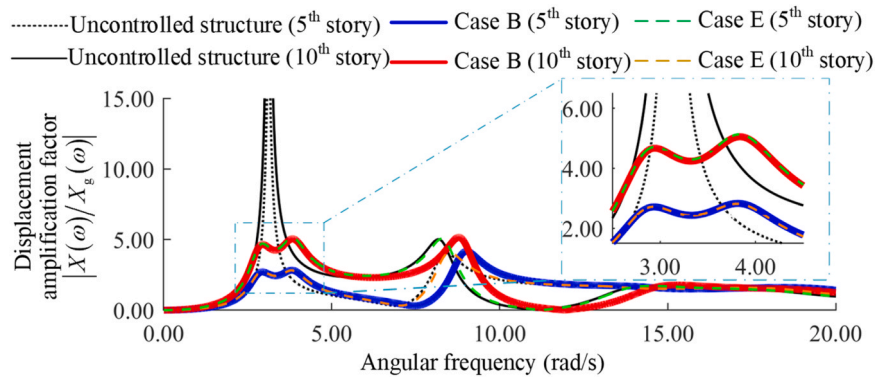


Fig. 13. Displacement amplification factor curves for the 10-story benchmark steel building without control, and with practical SPD-TVMD (Case B) and practical MPD-TVMD (Case E).

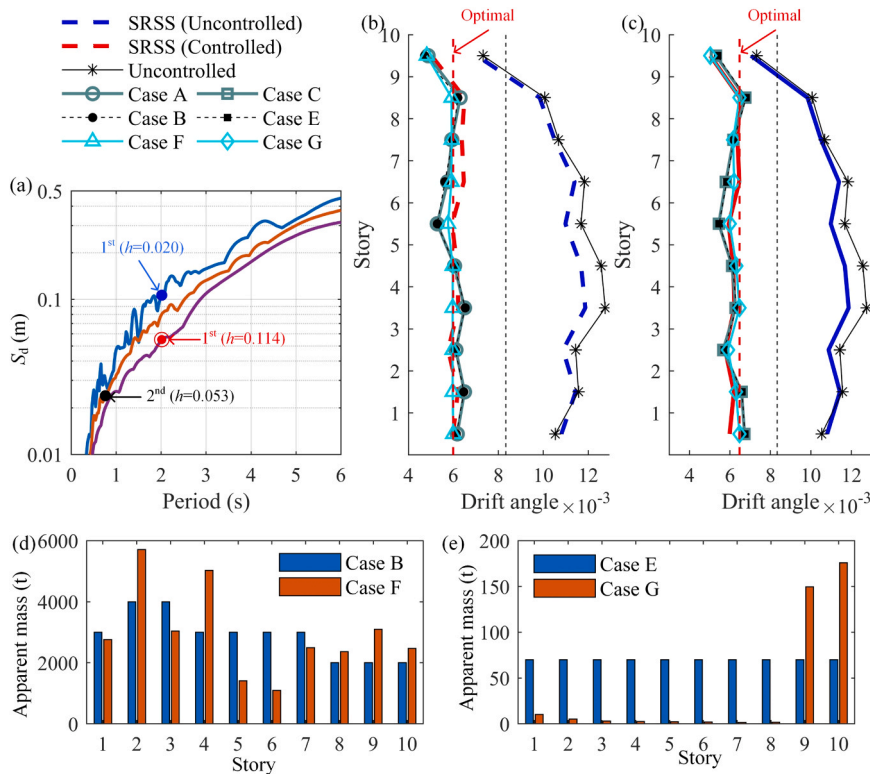


Fig. 14. Comparison of maximum structural displacement responses: (a) Spectral displacement response of an artificial earthquake wave considering damping ratios of 0.02, 0.053, and 0.114. (b) Comparison of maximum structural drift angles for Cases A, B and F estimated by time history analysis and the SRSS method. (c) Comparison of maximum structural drift angles for Cases C, E and G estimated by time history analysis and the SRSS method. (d) Apparent mass distribution comparison for Cases B and F. (e) Apparent mass distribution comparison for Cases E and G.

damping ratios. Fig. 14 (b) and (c) compare the maximum structural displacement responses estimated by the time history response analysis and the SRSS method. It can be observed that there is a considerable degree of consistency between the two methods. The slight discrepancies are mainly due to the SRSS method neglecting the coupling effects between modes. For comparison, the optimal damping effects, quantified by maximum drift angles, achievable by interstory-installed TVMDs (a general form of SPD-TVMD) and ground-installed TVMDs (a general form of MPD-TVMD), both with a mass ratio of  $\mu = 0.1$ , considering variations in distribution patterns, are depicted in Fig. 14 (b) and (c) as lines labeled Case F and Case G. The design parameters for Cases F and G were determined using a numerical optimization algorithm. The design variables included the apparent mass distribution of each story's TVMDs, along with the corresponding frequency ratio  $\beta$  and

damping ratio  $h_d$ . The objective was to minimize the maximum inter-story drift angle under the selected seismic wave. Fig. 14 (d) and (e) illustrate the optimal distribution of interstory and ground-installed TVMDs. It is observed that to maintain modal preservation characteristics, the damping performances of SPD-TVMD and MPD-TVMD are reduced by 8.3 % and 6.0 %, respectively, compared to the optimal cases. Nonetheless, given the design convenience offered by SPD-TVMD and MPD-TVMD, this trade-off is deemed acceptable.

### 5. Conclusion

This study examines the modal response characteristics of proportionally distributed TVMDs incorporated in an MDOF shear building. The main contributions of this study are summarized as follows.

- By constructing the modal participation vectors of MDOF systems controlled by SPD-TVMD and MPD-TVMD, it was demonstrated that the fundamental modes of the undamped primary system remain unchanged after the addition of SPD-TVMD and MPD-TVMD. Furthermore, the complex participation mode vectors of the controlled MDOF structure can be obtained by combining the participation mode vectors of the uncontrolled system with those of corresponding reduced 2-DOF systems.
- The analysis of 2-story and 10-story example structures containing SPD-TVMD and MPD-TVMD further verified numerically that these distribution patterns possess mode-preserving characteristic. A comparison of design parameters indicates that the MPD-TVMD configuration reduces the total apparent mass and damping coefficient requirements by over 60 % and 90 %, respectively, compared to the SPD-TVMD for the 2-story and 10-story structures. This demonstrates that the MPD pattern is highly efficient in utilizing TVMDs, albeit at the cost of requiring additional structural components, such as external braced frames.
- The analysis of a 10-story benchmark steel building containing SPD-TVMD demonstrated that the mode-preserving characteristic could be practically maintained even if the TVMDs did not strictly adhere to a stiffness-proportional distribution considering the practical design.
- The analysis of a 10-story benchmark steel building with an MPD-TVMD based external dissipative system demonstrated that by modifying the tuning spring stiffness to cancel the flexibility of the external braced frame that has the same stiffness as the primary structure, the mode-preserving characteristic of MPD-TVMD could be practically maintained.

Although this study focused only on TVMDs, it is expected that the conclusions drawn from this study can be applied to other types of inerter-based devices. This study solely considers the practical limitations encountered in engineering, where TVMDs may not be distributed in strict proportionality. It demonstrates that these constraints

minimally affect the modal preservation and control effectiveness of both SPD- and MPD-TVMD systems. Consequently, the implementation of SPD- and MPD-TVMD systems warrants further exploration with more realistic design considerations, including restrictions on the height of floor-to-ground device installations.

**CRedit authorship contribution statement**

**Liyu Xie:** Writing – review & editing, Writing – original draft, Investigation. **Chunfeng Wan:** Writing – review & editing, Writing – original draft, Validation. **Songtao Xue:** Writing – review & editing, Writing – original draft, Supervision, Funding acquisition. **Jianfei Kang:** Writing – review & editing, Writing – original draft, Visualization, Validation, Supervision, Software, Methodology, Investigation. **Zhipeng Zhao:** Writing – review & editing, Writing – original draft, Validation, Supervision, Software, Investigation, Funding acquisition, Formal analysis.

**Declaration of Competing Interest**

The authors declare that they have no known competing financial interests or personal relationships that could have appeared to influence the work reported in this paper.

**Acknowledgments**

The authors express their sincere gratitude to Professor Kohju Ikago of Tohoku University for his invaluable support in the completion of this study. This study was supported by the National Natural Science Foundation of China (Grant No. 52308525), National Key R&D Program of China (Grant No. 2021YFE0112200), the Natural Science Foundation of Shanghai (Grant No. 20ZR1461800), and the Fundamental Research Funds for the Central Universities (Grant No. 22120240428). All support is gratefully acknowledged.

**Appendix A**

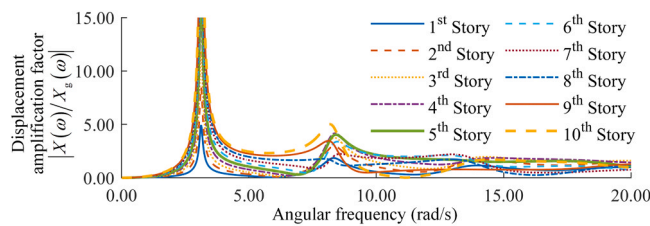


**Figure A.1.** Displacement amplification factor curves for each story of the 10-story uncontrolled benchmark steel building.

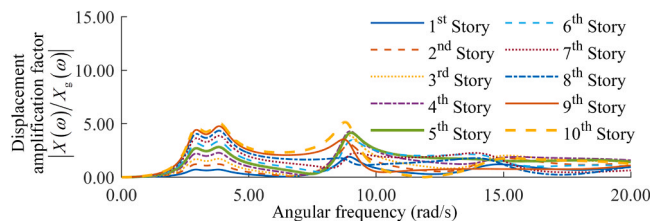


**Figure A.2.** Displacement amplification factor curves for each story of the 10-story benchmark steel building controlled by the practical SPD-TVMD (Case B).

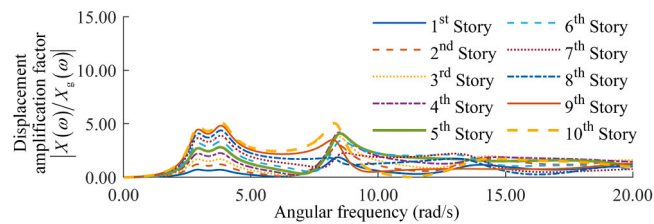


Figure A.3. Displacement amplification factor curves for each story of the 10-story benchmark steel building controlled by the practical MPD-TVMD (Case E).

## Data availability

Data will be made available on request.

## References

- Ikago K, Saito K, Inoue N. Seismic control of single-degree-of-freedom structure using tuned viscous mass damper. *Earthq Eng Struct Dyn* 2012;41:453–74. <https://doi.org/10.1002/eqe.1138>.
- Watanabe Y, Ikago K, Inoue N, Kida H, Nakaminami S, Tanaka H, et al. Full-scale dynamic tests and analytical verification of a force-restricted tuned viscous mass damper. *Proc 15th World Conf Earthq Eng, Lisbon, Port* 2012. ID 1206.
- Garrido H, Curadelli O, Ambrosini D. Improvement of tuned mass damper by using rotational inertia through tuned viscous mass damper. *Eng Struct* 2013;56:2149–53. <https://doi.org/10.1016/j.engstruct.2013.08.044>.
- Lazar IF, Neild SA, Wagg DJ. Using an inerter-based device for structural vibration suppression. *Earthq Eng Struct Dyn* 2014;43:1129–47. <https://doi.org/10.1002/eqe.2390>.
- Zhao Z, Hu X, Zhang R, Xie M, Liu S. Advantages and design of inerters for isolated storage tanks incorporating soil conditions. *Thin-Walled Struct* 2024;195:111356. <https://doi.org/10.1016/j.tws.2023.111356>.
- Zhao Z, Chen Q, Hu X, Zhang R. Enhanced energy dissipation benefit of negative stiffness amplifying dampers. *Int J Mech Sci* 2023;15:107934. <https://doi.org/10.1016/j.ijmecsci.2022.107934>.
- Pietrosanti D, De Angelis M, Basili M. A generalized 2-DOF model for optimal design of MDOF structures controlled by tuned mass damper inerter (TMDI). *Int J Mech Sci* 2020;185:105849. <https://doi.org/10.1016/j.ijmecsci.2020.105849>.
- Smith MC. Synthesis of mechanical networks: the inerter. *IEEE Trans Autom Control* 2002;47:1648–62. <https://doi.org/10.1109/TAC.2002.803532>.
- Kawamata S. Accelerated liquid mass damper and principles of structural vibration control. *Trans Int Conf Struct Mech React Technol, Lausanne* 1987:737–42.
- Kawamata S. Liquid type mass damper with elongated discharge tube. US4872649A, 1989.
- Fujinami T, Yamamoto S. Dynamic absorber using lever and pendulum mechanism for vibration control of structure. (the principle of mechanism and its optimum tuning). *Trans Jpn Soc Mech Eng Ser C* 1991;57:1842–7. <https://doi.org/10.1299/kikaic.57.1842>.
- Sone A, Yamamoto S, Masuda A. Sliding mode control for building using tuned mass damper with pendulum and lever mechanism during strong earthquake. *Proc 2nd World Conf Struct Control, Kyoto, Jpn* 1998:531–40.
- Okumura A. Vibration isolation connection device and structure vibration isolation connection mechanism. JP3718683B2, 2005.
- Okumura A. Multilayered vibration insulation connection mechanism. JP2005240839A, 2005.
- Saitoh M. On the performance of gyro-mass devices for displacement mitigation in base isolation systems. *Struct Control Health Monit* 2012;19:246–59. <https://doi.org/10.1002/stc.419>.
- Arakaki T, Kuroda H, Arima F, Inoue Y, Baba K. Development of seismic devices applied to ball screw: part 1 basic performance test of RD-series. *AIJ J Technol Des* 1999;5:239–44. <https://doi.org/10.3130/aijt.5.239>.
- Arakaki T, Kuroda H, Arima F, Inoue Y, Baba K. Development of seismic devices applied to ball screw: part 2 performance test and evaluation of RD-series. *AIJ J Technol Des* 1999;5:265–70. <https://doi.org/10.3130/aijt.5.265>.
- Sugimura Y, Goto W, Tanizawa H, Saito K, Ninomiya T, Nagasaku T. Response control effect of steel building structure using tuned viscous mass damper. *Proc 15th World Conf Earthq Eng, Lisbon, Port* 2012. ID 0138.
- Ogino M, Sumiyama T. Structural design of a high-rise building using tuned viscous mass dampers installed across three consecutive storeys. *Civ -Comp Proc, Naples, Italy* 2014:225. <https://doi.org/10.4203/ccp.106.225>.
- Hwang J-S, Kim J, Kim Y-M. Rotational inertia dampers with toggle bracing for vibration control of a building structure. *Eng Struct* 2007;29:1201–8. <https://doi.org/10.1016/j.engstruct.2006.08.005>.
- Liu X, Jiang JZ, Titurus B, Harrison A. Model identification methodology for fluid-based inerters. *Mech Syst Signal Process* 2018;106:479–94. <https://doi.org/10.1016/j.ymssp.2018.01.018>.
- Zhang X-L, Zhu Z, Nie J-M, Liao YG. Mem-inerter: a passive nonlinear element equivalent to the semi-active inerter performing initial-displacement-dependent inertance control strategy. *J Braz Soc Mech Sci Eng* 2021;43:574. <https://doi.org/10.1007/s40430-021-03282-0>.
- Wang F-C, Hong M-F, Lin T-C. Designing and testing a hydraulic inerter. *Proc Inst Mech Eng Part C J Mech Eng Sci* 2011;225:66–72. <https://doi.org/10.1243/09544062JMES2199>.
- Gonzalez-Buelga A, Clare L, Neild S, Jiang J, Inman D. An electromagnetic inerter-based vibration suppression device. *Smart Mater Struct* 2015;24:055015. <https://doi.org/10.1088/0964-1726/24/5/055015>.
- John EDA, Wagg DJ. Design and testing of a frictionless mechanical inerter device using living-hinges. *J Frankl Inst* 2019;356:7650–68. <https://doi.org/10.1016/j.jfranklin.2019.01.036>.
- Furuhashi T, Ishimaru S. Mode control seismic design with dynamic mass. *Proc 14th World Conf Earthq Eng, Beijing, China* 2008. ID 11-0028.
- Kaynia AM, Veneziano D, Biggs JM. Seismic effectiveness of tuned mass dampers. *J Struct Div* 1981;107:1465–84. <https://doi.org/10.1061/JSDEAG.0005760>.
- Radu A, Lazar IF, Neild SA. Performance-based seismic design of tuned inerter dampers. *Struct Control Health Monit* 2019;26:e2346. <https://doi.org/10.1002/stc.2346>.
- Zhang R, Zhao Z, Pan C, Ikago K, Xue S. Damping enhancement principle of inerter system. *Struct Control Health Monit* 2020;27:e2523. <https://doi.org/10.1002/stc.2523>.
- Krenk S, Høgsberg J. Tuned resonant mass or inerter-based absorbers: unified calibration with quasi-dynamic flexibility and inertia correction. *Proc R Soc Math Phys Eng Sci* 2016;472:20150718. <https://doi.org/10.1098/rspa.2015.0718>.
- David H. Damping of torsional beam vibrations: PhD thesis. PhD Thesis. Technical University of Denmark, 2019.
- Tafianidis AA, Giaralis A, Patsialis D. Multi-objective optimal design of inerter-based vibration absorbers for earthquake protection of multi-storey building structures. *J Frankl Inst* 2019;356:7754–84. <https://doi.org/10.1016/j.jfranklin.2019.02.022>.
- Wen Y, Chen Z, Hua X. Design and evaluation of tuned inerter-based dampers for the seismic control of MDOF structures. *J Struct Eng* 2017;143:04016207. [https://doi.org/10.1061/\(ASCE\)ST.1943-541X.0001680](https://doi.org/10.1061/(ASCE)ST.1943-541X.0001680).
- Zhang R, Wu M, Pan C, Wang C, Hao L. Design of MDOF structure with damping enhanced inerter systems. *Bull Earthq Eng* 2022. <https://doi.org/10.1007/s10518-022-01381-4>.
- Prakash S, Jangid RS. Optimum parameters of tuned mass damper-inerter for damped structure under seismic excitation. *Int J Dyn Control* 2022;10:1322–36. <https://doi.org/10.1007/s40435-022-00911-x>.
- Islam NU, Jangid RS. Optimum parameters of tuned inerter damper for damped structures. *J Sound Vib* 2022;537:117218. <https://doi.org/10.1016/j.jsv.2022.117218>.
- Djerouni S, Abdeddaim M, Elias S, Rupakhety R, Djerouni S, Elias S, et al. Optimum double mass tuned damper inerter for control of structure subjected to ground motions. *J Build Eng* 2021;44:103259. <https://doi.org/10.1016/j.jobe.2021.103259>.
- Djerouni S, Elias S, Abdeddaim M, Domenico DD. Effectiveness of optimal shared multiple tuned mass damper inerters for pounding mitigation of adjacent buildings. *Pr Period Struct Des Constr* 2023;28:04022063. [https://doi.org/10.1061/\(ASCE\)SC.1943-5576.0000732](https://doi.org/10.1061/(ASCE)SC.1943-5576.0000732).
- Mazza F, Vulcano A. Control of the earthquake and wind dynamic response of steel-framed buildings by using additional braces and/or viscoelastic dampers. *Earthq Eng Struct Dyn* 2011;40:155–74. <https://doi.org/10.1002/eqe.1012>.
- Mazza F, Vulcano A. Displacement-based design procedure of damped braces for the seismic retrofitting of r.c. framed buildings. *Bull Earthq Eng* 2014;13:2121–43. <https://doi.org/10.1007/s10518-014-9709-7>.
- Bruschi E, Quaglino V, Calvi PM. A simplified design procedure for seismic upgrade of frame structures equipped with hysteretic dampers. *Eng Struct* 2022;251:113504. <https://doi.org/10.1016/j.engstruct.2021.113504>.
- Ikago K, Sugimura Y, Saito K. Simple design method for a tuned viscous mass damper seismic control system. *Proc 15th World Conf Earthq Eng, Lisbon, Port* 2012. Paper ID 1575.
- Ikago K, Sugimura Y, Saito K, Inoue N. Modal response characteristics of a multiple-degree-of-freedom structure incorporated with tuned viscous mass

- dampers. *J Asian Arch Build Eng* 2012;11:375–82. <https://doi.org/10.3130/jaabe.11.375>.
- [44] Xue S, Kang J, Xie L, Zhang R, Ban X. Cross-layer installed cable-bracing inerter system for MDOF structure seismic response control. *Appl Sci* 2020;10:5914. <https://doi.org/10.3390/app10175914>.
- [45] Kang J, Xue S, Xie L, Tang H, Zhang R. Multi-modal seismic control design for multi-storey buildings using cross-layer installed cable-bracing inerter systems: part 1 theoretical treatment. *Soil Dyn Earthq Eng* 2023;164:107639. <https://doi.org/10.1016/j.soildyn.2022.107639>.
- [46] Trombetti T, Silvestri S. Added viscous dampers in shear-type structures: the effectiveness of mass proportional damping. *J Earthq Eng* 2004;8:275–313. <https://doi.org/10.1080/13632460409350490>.
- [47] Trombetti T, Silvestri S. On the modal damping ratios of shear-type structures equipped with rayleigh damping systems. *J Sound Vib* 2006;292:21–58. <https://doi.org/10.1016/j.jsv.2005.07.023>.
- [48] Trombetti T, Silvestri S. Novel schemes for inserting seismic dampers in shear-type systems based upon the mass proportional component of the rayleigh damping matrix. *J Sound Vib* 2007;302:486–526. <https://doi.org/10.1016/j.jsv.2006.11.030>.
- [49] Saito K, Sugimura Y, Nakaminami S, Kida H, Inoue N. Vibration tests of 1-story response control system using inertial mass and optimized soft spring and viscous element. *Proc 14th World Conf Earthq Eng*, Beijing, China 2008.
- [50] Chopra AK. *Dynamics of structures*. 5th edition... Upper Saddle River, N.J: Pearson Education Limited; 2019.
- [51] Strang G. *Introduction to linear algebra*. 5th edition., Wellesley: Wellesley-Cambridge Press; 2016.
- [52] *JSSI Manual*. Design and construction manual for passively controlled buildings. 2nd edition., Tokyo, Japan: Japan Society of Seismic Isolation; 2005.
- [53] Zhang R, Zhang L, Pan C, Chen Q, Wang Y. Generating high spectral consistent endurance time excitations by a modified time-domain spectral matching method. *Soil Dyn Earthq Eng* 2021;145:106708. <https://doi.org/10.1016/j.soildyn.2021.106708>.
- [54] GB 50011–2010. Code for seismic design of the buildings, National Standard of the People's Republic of China. Ministry of Housing and Urban-Rural Development of the People's Republic of China; Beijing, China: 2016.